Biomedicine & Pharmacotherapy 194 (2026) 118913

Contents lists available at ScienceDirect

Biomedicine & Pharmacotherapy

journal homepage: www.elsevier.com/locate/biopha

GPRASP1 deletion suppresses antinociceptive tolerance during chronic activation of delta opioid receptor in persistent pain

Juliette Kaeffer [a], Marie-Laure Straub [a], Glenn-Marie Le Coz [a], Raphaëlle Quillet [a], Valérie Kugler [a], Nathalie Petit-Demoulière [a], Manon Gerum [a], Gabrielle Zeder-Lutz [a], Stéphane Doridot [b], Michael Dumas [a], Johana Chicher [c], Philippe Hammann [c], Philippe Marin [d], Franck Vandermoere [d], Dominique Massotte [e], Frédéric Simonin [a,1], Sandra Lecat [a,1,*]

[a] Biotechnologie et Signalisation Cellulaire, UMR7242, CNRS, Université de Strasbourg, Illkirch, France
[b] Chronobiotron, UAR3415, Université de Strasbourg, France
[c] Plateforme de protéomique, FR1589 Institut de biologie moléculaire et cellulaire IBMC, CNRS, France
[d] Institut de Génomique Fonctionnelle, Université de Montpellier, CNRS, Inserm, France
[e] UPR3212 Institut des neurosciences cellulaires et intégratives (INCI) CNRS, France

ARTICLE INFO

Keywords:
Delta opioid receptor
G protein-coupled receptor
Pain
Tolerance
GPCR-associated sorting protein

ABSTRACT

Delta-opioid receptor (DOR) agonists display antinociceptive properties with less adverse effects than morphine derivatives and other opioids targeting mu-opioid receptor. However, a loss of their antinociceptive effect (tolerance) rapidly develops upon repeated treatments and could be due to the fast degradation of DOR. The G Protein-coupled Receptor-Associated Sorting Protein 1 (GPRASP1) has been involved in DOR sorting for degradation *in vitro*. Here, using a novel mouse line combining a knock-out for GPRASP1 and a knock-in for a fluorescent DOR-eGFP, we show that GPRASP1 is mandatory for the development of antinociceptive tolerance to the DOR agonist SNC80 in models of neuropathic and inflammatory pain. Surprisingly, DOR down-regulation upon repeated activations, phosphorylation kinetics of SNC80-activated DOR and DOR coupling to Gi proteins were unaffected by the loss of GPRASP1. Instead, changes in the dynamics of DOR plasma membrane localization were observed in GPRASP1 knockout neurons. Affinity-Purification of DOR followed by Mass Spectrometry analyses revealed, for the first time in the brain, that SNC80 alters DOR's interactome. In the absence of GPRASP1, the association of activated DOR with newly identified partners, particularly Synapse differentiation-inducing gene protein 1 SYNG1, was reduced. These findings indicate that SNC80-induced antinociceptive tolerance is not driven by DOR down-regulation but rather by GPRASP1-mediated changes in DOR trafficking and downstream signaling.

1. Introduction

Chronic pain is a serious health issue that concerns 20 % of adults in Western countries [1]. For around 5–8 % of people, it is subcategorized as High-Impact chronic pain [2–4] because it has various psychological impacts and becomes disabling in daily life. Among the G Protein-Coupled Receptors (GPCRs) involved in the establishment and maintenance of chronic pain, opioid receptors and particularly mu opioid receptor (MOR), the receptor of drugs like morphine and its derivatives and of synthetic opioids such as fentanyl and methadone, are still considered as major targets for its treatment [5–8].

In line with its involvement in regulation of nociception, the delta opioid receptor (DOR) could be an alternative drug target for the treatment of chronic pain [9]. DOR is located in different regions of the nervous system involved in the modulation of nociception and pain, including the dorsal root ganglia, spinal cord, striatum and amygdala. Like MOR, it is coupled to $G_{i/o}$ proteins and reduces the transmission of nociceptive signals [10]. Studies on animal models of chronic pain of

* Correspondence to: Biotechnologie et Signalisation Cellulaire, UMR7242, CNRS, Université de Strasbourg, 300 Bld Sébastien Brant, Illkirch 67412, France.
E-mail address: lecat@unistra.fr (S. Lecat).
[1] Co-senior authors

https://doi.org/10.1016/j.biopha.2025.118913
Received 16 July 2025; Received in revised form 9 December 2025; Accepted 16 December 2025

various etiologies (neuropathic, inflammatory, cancer and diabetic) have shown that DOR stimulation with agonists prevents both mechanical and thermal hyperalgesia [11]. DOR agonists do not induce side-effects of MOR agonists such as constipation or respiratory depression, and display low addictive properties [12]. However, one of the main limitations of the use of DOR agonists, such as SNC80 (a prototypical DOR agonist promoting fast receptor internalization), is the rapid development of an antinociceptive tolerance following their daily administration [13,14].Tolerance refers to the reduction of the effect of a drug upon successive administrations. Analgesic tolerance to MOR agonists appears to depend upon two processes, namely *i)* cellular tolerance that includes mechanisms such as the decrease in functional MORs caused by their desensitization and internalization through β-arrestins, and the reinforcement of counteracting signaling, such as over-activation of the adenylyl cyclase; and *ii)* adaptive modifications of the pain circuitry of the nervous system and development of opioid-induced hyperalgesia [15–17]. Antinociceptive tolerance to MOR agonists is ligand-dependent and much effort has been directed towards developing biased agonists that poorly activate the β-arrestin pathways and thereby induce less tolerance [18,19]. Although a rapid degradation of DOR in lysosomes [13,14,16] following its internalization by β-arrestin1 [20,21] has been suggested to represent a critical step, the molecular mechanisms underlying the development of antinociceptive tolerance to DOR agonists are less well characterized.

One of the main proteins thought to be involved in DOR degradation *in vitro* is the GPCR-associated Sorting protein 1 (GPRASP1). Two-hybrid screens have identified an interaction between the carboxyl-terminal domains of GPRASP1 and DOR [22,23] further confirmed by pull-down assays [22–24] and by co-immunoprecipitation *in vitro* [22–25]. Pull-down assays also revealed that GPRASP1 interacts with the C-terminal domain of a large number of GPCRs [22,24]. Overexpression of GPRASP1 in Human Embryonic Kidney (HEK293) cells was shown to increase ligand-induced DOR degradation, as assessed by radioligand binding experiments [23]. GPRASP1 has been further implicated in degradation of GPCRs *in vitro* including the degradation of the dopamine D2 and D3 receptors [26,27] and DOR via interactions with the Hepatocyte growth factor-regulated tyrosine kinase substrate (HGS) component of the Endosomal Sorting Complex Required for Transport (ESCRT-0) protein complex and dysbindin [28,29] as well as the degradation of the cannabinoid receptor (CNR1) [30,31] via an interaction with Beclin2 [32,33]; for review see [34,35].

Several teams have independently generated GPRASP1-deficient mice [36–39] and have studied their behavior as well as the degradation of different receptors upon their repeated stimulation. Converging results clearly establish the requirement of GPRASP1 for adaptations following repeated activations of D2 and D3 receptors [36–38] or of β2-adrenoceptors [40] and in the development of antinociceptive tolerance to agonists targeting CNR1 [41]. However, conflicting results have been reported concerning degradation of GPCRs upon repeated activations in GPRASP1 KO mice [35–37,40,41] indicating that the role of GPRASP1 in chronic stimulation of GPCRs still needs clarification.

While DOR was the first GPCR shown to interact with GPRASP1 *in vitro*, no study has been undertaken to understand its role in DOR signaling and trafficking *in vivo*. Here, we used a novel mouse line combining a knock-out (KO) for GPRASP1 [36] and expressing a knock-in (KI) fluorescent DOR fused at its cytoplasmic C-terminal tail with the enhanced Green Fluorescent Protein (eGFP) [14,42–45] in models of persistent pain to explore the mechanism of antinociceptive tolerance induced by repeated activations of DOR and to track the cell fate of the receptor. We now demonstrate that GPRASP1 is required for the development of antinociceptive tolerance to SNC80 by a mechanism independent of both DOR down-regulation and coupling to heterotrimeric Gi/o proteins, strengthening its potential as a new drug target. We further identified novel DOR-interacting partners modulated by GPRASP1 expression as other candidates implicated in the development of tolerance.

2. Material and methods

2.1. Compounds

The Complete Freund's Adjuvent (CFA, F5881) and Naltrexone hydrochloride (N3136) were obtained from Sigma Aldrich. Naltrindole hydrochloride (HY-101177) and SNC 80 (07829 J), were obtained from Interchim (Cayman chemical company, Ann Arbor, MI, USA). Radioactive [^{3}H]-Deltorphine II was synthetized by Perkin Elmer (NET1087959UC)

2.2. Engineering of DOR-eGFP/GPRASP1 KO mice

DOR-eGFP/GPRASP1 KO mice were obtained by crossbreeding DOR-eGFP KI mice [44] and GPRASP1 KO mice [36] (See Supplementary data and methods). All mice used in this study were C57/Bl6/J: 129svPas (50:50 %). All experiments were carried out in strict accordance with the European guidelines for the care of laboratory animals (European Communities Council Directive 2010/63/EU) and approved by the local ethical committee APAFIS#26036–202006010931233 v5. All efforts were made to minimize animal discomfort and to reduce the number of animals. Our study examined male and female animals in the neuropathic pain model and similar findings in this pain model are reported for both sexes.

2.3. Neuropathic pain model and assessment of mechanical and cold allodynia

Before the surgery, mice were given two weeks to acclimatise to the experimental device then basal thresholds for mechanical and thermal sensitivity were evaluated during 5 consecutive days from day minus 26 (D-26) to day minus 21 (D-21). Neuropathic pain was induced by chronic constriction injury (CCI) on the main branch of the right sciatic nerve, as described in [46] (Supplementary data and methods). Animals were 8–18 weeks old on the day of the surgery, n = 10–12 per group.

Mechanical allodynia (AD) was assessed with a series of eight von Frey filaments (VF, Bioseb, Vitrolles, France), according the up & down method [47,48]. Briefly, calibrated VF filaments with the bending force of 0.008–2 g were applied on the hind paw, starting at 0.4 g. Depending on whether the animal responded to this stimulation, the higher or lower grammage filament was tested next. The response/non-response sequence was used to determine a sensitivity threshold. Contralateral paw was used as internal control. Cold allodynia was evaluated with a cold plate apparatus (CP). Mice were placed 5 min on a plate cooled to 4°C, from which they cannot escape, and each paw lift was scored [49].

2.4. Inflammatory pain model and assessment of mechanical and thermal hyperalgesia

Mice were accustomed to the manipulation and the test device during one week. The basal nociceptive threshold of the animals was then measured daily for 5 days from day minus 7 (D-7) to day minus 3 (D-3). To induce an inflammatory pain, CFA was injected at the base of the tail (20 μL, sub-cutaneously (s.c.) in the caudal region, 1 cm from the base, using a 24 G needle with Hamilton syringe, adapted from [13,50]. The development of hyperalgesia was observed 72 h after the CFA injection.

Mechanical hyperalgesia (HA) was evaluated with the tail pressure test (TPT) with an instrumented rodents' pincher (RP1, Bioseb). A gradual pressure was applied to the base of the tail, near the site where the inflammatory agent was injected until the animal removes its tail, indicating the pressure necessary to induce a withdrawal reflex of the tail. Baseline was typically around 200 g allowing to visualize the hyperalgesia in a significant manner 72 h post-CFA. Thermal hyperalgesia was assessed by the tail immersion test (TIT). The distal two-thirds of the mouse tail were placed in water at 46.5 ± 0.5 °C [13,50]. The time taken to observe the tail withdrawal reflex was monitored. The

temperature of the waterbath was adjusted in order to have a baseline threshold around 10 sec allowing to visualize the hyperalgesia in a significant manner 72 h post-CFA. The cut-offs were defined as three times the average baseline threshold according to the International Association for the Study of pain (IASP) recommendations therefore of around 600 g in the TPT and 30 sec in the TIT. All measures were done in triplicates during baseline and in duplicate during testing, mechanical and thermal nociception were evaluated on the same animals on the same day, as we have observed very reproducible results for this one time-point analysis in animals and that no pain sensitization was observed following this procedure.

Animals were either non-fluorescent DOR (Fig. S3B, *C*, *E*, *F*), homozygotes for DOR-eGFP (Fig. 1*E*, *F*, FigS3A, *D*, *G*, *H*) or a mix of heterozygotes and homozygotes for DOR-eGFP (Fig. 1*C*, *D*). They were 8–22 weeks old on the day of CFA injection.

2.5. In vivo evaluation of antinociceptive effects of SNC80

Animals were divided according to genotypes in groups equilibrated for baseline nociception. Allodynia or hyperalgesia were verified by adequate tests. Agonist treatment was performed when allodynia or hyperalgesia were established (significant differences with baseline nociceptive threshold). The agonist SNC80 was diluted in saline solution (NaCl 0.9 %) and placed in acidic conditions (6 mM HCl) at a concentration of 1 mg/mL [14,21,51].

In the neuropathic pain model, SNC80 was administered intraperitoneally (i.p.) once a day up to 9 days in males in a first experiment. Nociceptive threshold was evaluated 45 min after each SNC80 administration as in [14]. Mechanical allodynia was measured daily by Von frey's tests (VF) and for cold allodynia, only one test on cold plate (CP) was performed, after mechanical antinociceptive tolerance in WT mice was established. In the neuropathic pain model, mechanistic differences between females and males have been reported [52–54]. We therefore generated females in a subsequent crossing of mice since the GPRASP1

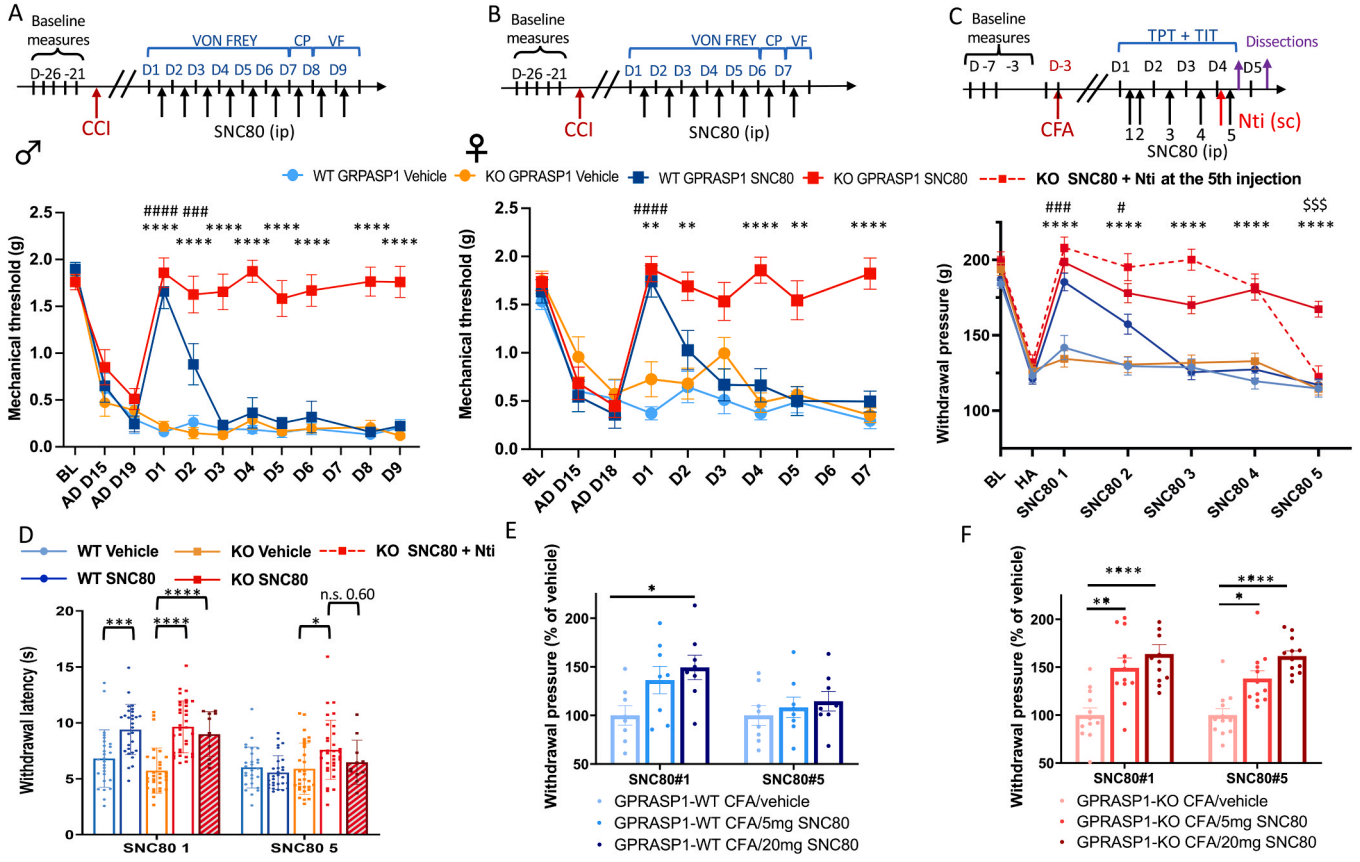

Fig. 1. Absence of antinociceptive tolerance in DOR-eGFP/GPRASP1 KO mice: neuropathic and inflammatory pain models. The experimental designs are depicted above each graph of the corresponding experiment in A, B, C. (**A, B**) After baseline mechanical threshold measurements (BL) for five days with Von Frey's filaments (VF, D-26 to D-21), mice received chronic constriction injury (CCI) surgery of the right paw (red arrow). Allodynia (AD) was verified on day 15 (D15) and day 19 (D19) post-surgery. The anti-allodynic effect of SNC80 was investigated once a day 45 min after its administrations starting from day 1 (D1) (black arrows, 10 mg/kg i.p.). Values are expressed as mean± SEM of n = 12 WT male mice, n = 11 GPRASP1 KO male mice, n = 11–12 WT female, n = 10 GPRASP1 KO female mice. (**C, D**) After baseline (BL) mechanical and thermal threshold measurements by tail pressure test TPT (C) and tail immersion test TIT (D) for five days (D-7 to D-3), inflammation was induced by CFA injection 1 cm from the base of the tail of male mice at D-3. Hyperalgesia (HA) was verified on Day 1. The anti-hyperalgesic effect of SNC80 was investigated 45 min after its administrations starting from Day 1 (D1) with two consecutive SNC80 administrations at 4 h intervals followed by one daily administration up to 5 injections of agonist in total (black arrows, 10 mg/kg i.p.). Values are expressed as mean ± SEM (C) or individual values with means ± SEM (D) of n = 30–31 WT mice, n = 36 GPRASP1 KO mice. Selective antagonist naltrindole administration (Nti, red arrow, 5 mg/kg s.c., 20 min prior the last SNC80 injection (dashed red line in C, dashed histogram in D, n = 11 GPRASP1 KO mice). Brains and spinal cord were collected by dissection after the last administration of SNC80 (C purple arrows). (**E, F**) Dose-response of the antinociceptive effect of SNC80 (5 or 20 mg/kg, i.p.) in the inflammatory pain model. The mechanical modality was evaluated in the same experimental design than in (C) by the TPT, WT mice (E) and in GPRASP1 KO mice (F). Values are expressed as individual values with means ± SEM of n = 8 for WT and n = 12 for GPRASP1 KO. Statistical analyses performed by two-way ANOVA followed by a Tukey's multiple comparison post hoc test. In A, B, C; WT vehicle vs WT SNC80: $^{###}$ P < 0.0005; $^{#}$ P < 0.05. KO vehicle vs KO SNC80: **** P < 0.0001, KO SNC80 vs KO Nti SNC80: $^{\$\$}$ $^{\$}$ P < 0.0005. In D, E, F, G : SNC80 compared to vehicle * P < 0.05; *** P < 0.0005; **** P < 0.0001.

gene is on the X chromosome. Female were then tested in a second cohort, for which the repeated SNC80 treatment was shortened to 7 days since no development of antinociceptive tolerance was observed in GPRASP1 KO mice at each SNC80 injection, while tolerance was established on day 3 onwards in WT mice.

In the inflammatory pain model, no difference between sex has been observed previously concerning the extent of anti-nociceptive effect of SNC80 administration or the development of tolerance upon a repeated SNC80 treatment [20,21]. In male mice, two injections of SNC80 were performed at four-hour intervals on day 1 to precipitate antinociceptive tolerance according to [13,20,21], and then once a day up to 4 days. Nociception was measured by tail pressure and tail immersion tests (TPT and TIT respectively). The CFA model experiments were conducted in three independent experiments of n = 10–12 male mice per groups: experiment 1 was performed with one dose of SNC80 (10 mg/kg, i.p.) followed by the dissection of brains and lumbar spinal cords 5 h after the last behavioral test. Experiment 2 was performed with three doses of SNC80 (5–10–20 mg/kg, i.p.) followed by the dissection of brain 24 h after the last behavioral test. Experiment 3 was performed with mice treated with repeated SNC80 injections, but 20 min prior to the 5th injection of SNC80 in GPRASP1 KO mice, Naltrindole (5 mg/kg, s.c,) was administered as described in [55]. This selective DOR antagonist was used to confirm that antinociception triggered by SNC80 in GPRASP1 KO mice occurred through the activation of DOR.

2.6. Behavioral data analysis

Statistical analyses were performed with GraphPad Prism v5 (GraphPad, San Diego, CA, USA). Two-way ANOVA (treatment genotype) analysis was used to compare the antinociceptive effect of SNC80 and tolerance development. One-way ANOVA analysis with multiple comparison followed by Tukey's *post hoc* analysis was performed to compare changes between SNC80 treated groups and vehicle from GPRASP1 wild-type (WT) and GPRASP1 KO mice.

2.7. Dissections

Brains and spinal cords were collected 4 h or 24 h after the last behavioral measurement. For the biochemical analysis that needed lysis of the tissues (radioligand binding, Western blot, immunoprecipitation), mice were killed by cervical dislocation and their brain was collected. Using large scissors, the spine was cut between T7 and L5 and the lumbar spinal cord was collected by Phosphate buffer saline (PBS, 137 mM NaCl; 2,7 mM KCl; 4,3 mM Na_2HPO_4 2 H_2O; 1,4 mM KH_2PO_4; pH = 7,4) flushing. Organs were frozen on dry ice as soon as possible and stored at −80°C. For immunohistochemical section imaging experiments, mice were anesthetized by intraperitoneal injection of ketamine/xylazine (100 mg/kg of Imalgène 1000 Boehringer Ingelheim Animal Health, Lyon, France + 10 mg/kg of Rompun 2 %; Bayer HealthCare, Kiel Germany, respectively) and perfused intracardiacally with flow rate of 10 mL/min, during 2 min with PBS to remove blood from the vascular system. Then tissues were fixed with PFA, 4 % (from EM-15714-S 32 %, Electron Microscopy Sciences, Hatfield, UK) diluted in 1x PBS, for 5 min. Organs were post-fixed in the same PFA solution for 24 h, cryoprotected in sucrose (30 % diluted in PBS) for 24 h at 4°C before being embedded in Cryomatrix (Optimal Cutting Temperature medium, N°6769006, Thermo scientific, UK) and kept frozen at −80°C.

2.8. Quantification of DOR-eGFP from brain membranes by radiolabeled binding experiments

To proceed to quantification of DOR binding sites, ^{3}H-Deltorphin II and 100 µg of brain membranes (see **Total membrane preparation** in Supplementary data and methods) were incubated in binding buffer (50 mM Tris HCl, 1 mM EDTA) in absence or presence of 1 µM naltrexone hydrochloride during 2 h at 25°C under agitation. The receptor-ligand complexes were filtered as described in [49] using a cell harvester apparatus (Brandel, Alpha Biotech Ltd, London, UK), on a glass fiber filters (Whatman GF/B; GE Healthcare, Saclay, France) pre-incubated with a polyethyleneimine solution containing 50 mM Tris HCl pH 7,4 and 0,5 % PEI (P3143, Sigma Aldrich, Saint-Louis, USA). Filters were then placed in scintillation counting vial (S207–5, Snap Twist, Simport, Beloeil, Quebec, Canada) with 2,5 mL of scintillation cocktail (Ultima Gold, 6013159, Perkin Elmer, Boston, MA, USA). After 12 h of incubation the radioactivity in each tube was quantified by scintillation counting on a Tricarb 4810 apparatus. To determine the maximum of possible binding (Bmax), a range of concentrations of ^{3}H-Deltorphin II from 0,09 nM to 6,4 nM was used. Background was determined with 1 µM naloxone hydrochloride. Once the Bmax determined by extrapolation of the saturation curve (on GraphPad Prism), samples from animals used for dose-effect evaluation were tested at a single saturating concentration of ^{3}H-Deltorphin II (4 nM). Animals were males, either WT non-fluorescent DOR (Fig. S4A), homozygotes for DOR-eGFP (Fig. S4B), heterozygotes for DOR-eGFP (Fig. 2*A*, left panel) or a mix of heterozygotes and homozygotes for DOR-eGFP (Fig. 2*A*, right panel). When a combination of heterozygotes and homozygotes for DOR-eGFP animals were used, DOR quantities were normalized to vehicle-treated GPRASP1-WT mice of the same genotype.

2.9. Quantification of DOR-eGFP from spinal cord lysates followed by immunoprecipitation

Spinal cords were kept frozen at −80°C until the lysis. Tissue weight was between 10 and 20 mg and lysis was performed in 350 µL of lysis buffer without detergents (50 mM tris HCl pH7,4, 150 mM NaCl, protease inhibitors (Complete, Roche, N°11873580001)). 5 ceramic beads (1,4 mm in diameter) were used to grind each spinal cord at 4°C by 2 cycles of 12 sec at 4260 rpm in Bioprep-24R (Allsheng) with a 5 sec interruption in between. The lysates were then centrifuged at 4°C for 10 min at 500 g. The supernatant was collected and detergents were added according to the supernatant volume (1 % Nonidet P40, 0,25 % sodium deoxycholate, 0,1 % sodium dodecylsulfate (SDS) and the volume of each sample was then completed to 1.2 mL with complete lysis buffer (50 mM tris HCl pH7,4, 150 mM NaCl, 1 % Nonidet P40, 0,25 % sodium deoxycholate, 0,1 % sodium dodecylsulfate (SDS) containing protease inhibitors (Complete, Roche, N°: 11873580001). The protein concentration was quantified by the BCA method, according to manufacturer instructions. 0.5 mg of proteins from one mouse were then mixed with 15 µl anti-GFP-Trap agarose beads (GTA-20, Chromotek) previously washed then conditioned with the lysis buffer. DOR-eGFP immunoprecipitations were carried out for 16 h on a turning wheel at 4°C. On the following day, the beads were collected after centrifugation at 5 min at 2500 g at 4°C. Three washes of 1 mL ice-cold Wash buffer (50 mM tris HCl pH7,4, 150 mM NaCl, 1 % Nonidet P40, 0,25 % sodium deoxycholate, 0,1 % sodium dodecylsulfate (SDS) without protease inhibitors) were done.

2.10. Western blot analysis of brain membranes or of immunoprecipitated DOR-eGFP

Samples from 50 µg of brain membranes or immunoprecipitations (total amount for spinal cord samples, or 12,5 % from co-immunoprecipitation of brain extracts) were resolved by SDS-PAGE. Samples were mixed to 4X Laemmli buffer (50 mM Tris pH 6,8, 6 M urea, 6 % beta-mercaptoethanol, 3 % SDS) to obtain a final concentration of 1X Laemmli buffer, shaked for 15 min and heated for 3 min at 95°C just before being loaded on 1.5 mm, 10 % acrylamide gels. Proteins were transferred onto PVDF membranes (Immobilon R P, Membrane PVDF 0,45 µm, IPVH00010, Merk Millipore, Darmstadt, Germany) by electrotransfer at 30 V and 4°C in transfer buffer (25 mM Tris HCl pH 7,4; 192 mM glycine; 0,01 % SDS, 10 % Ethanol) overnight. Membranes were then saturated in PBS containing 0,1 % Tween and 5 %

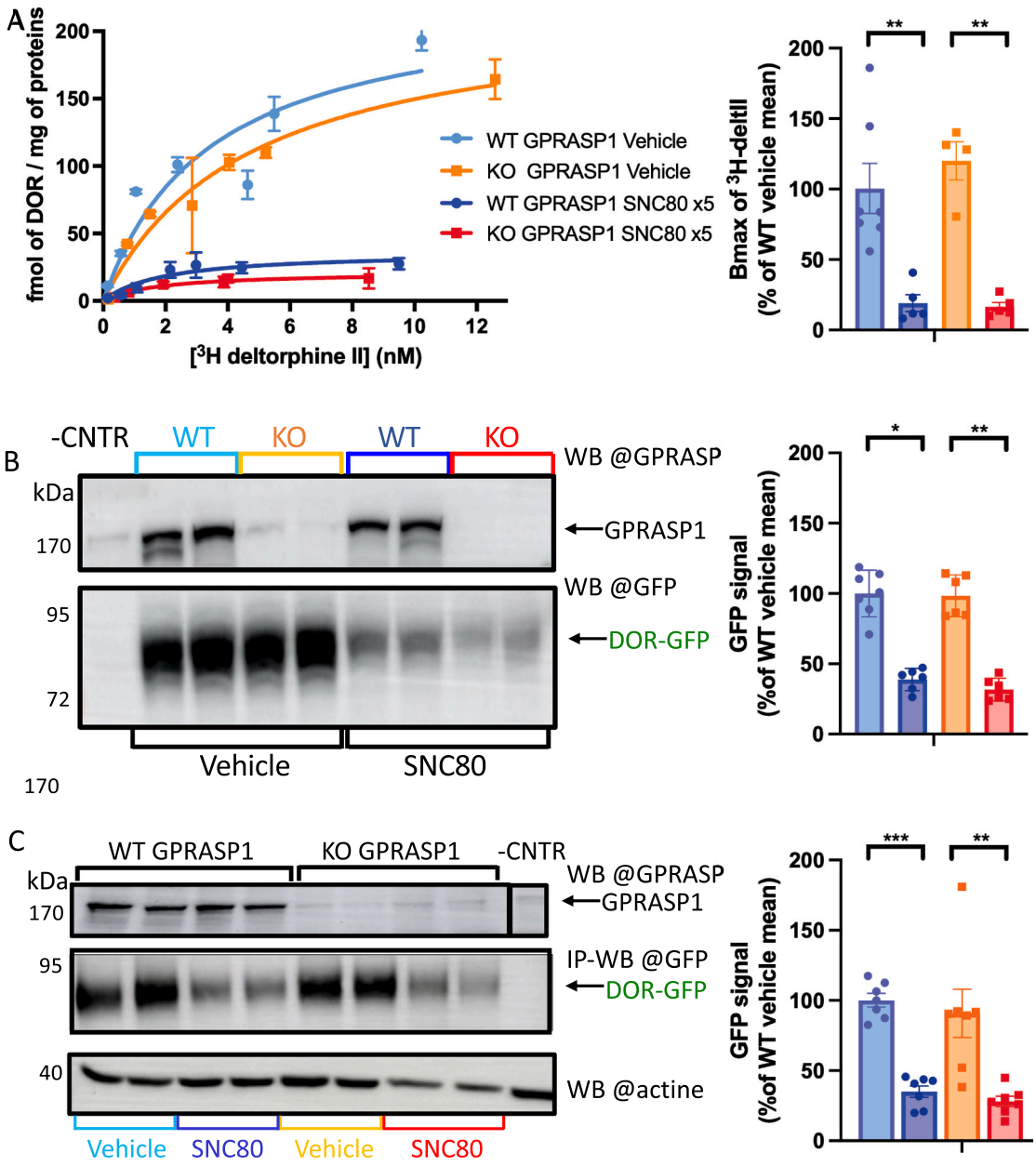

Fig. 2. Down-regulation of SNC80-activated DOR-eGFP is similar in both WT and GPRASP1 KO mice. (**A**, **B**, **C**) Quantifications of DOR-eGFP amount: In brain membranes, the DOR quantification was performed by two techniques, radiolabeling binding (A) or Western Blot (WB) (B). In spinal cord lysates, DOR quantification was performed by immunoprecipitation with GPF-trap beads (IP) followed by Western Blot (C). Brains and lumbar spinal cords of CFA-inflamed WT and GPRASP1 KO male mice treated with vehicle or SNC80 were dissected 5 h after the fifth injection of SNC80. (**A**) Left: Representative saturation curves of DOR quantification in brain membranes using ^{3}H-deltorphin II radiolabeled selective ligand for one animal in triplicates. Right: The amount of DOR determined by specific binding with 4 nM of ^{3}H-deltorphin II was expressed as % of the mean value of DOR quantity in WT-vehicle animals. (**B**) Left: Representative Western blots to detect GPRASP1 and DOR-eGFP from 50 µg of brain membranes. Each lane represents protein extracts from one mouse. DOR-eGFP was detected using anti-GFP-HRP antibodies. Actine was detected with anti-actine antiboby, GPRASP1 with anti-GPRASP antibodies. Right: Quantification of the GFP signal as % of the mean relative luminescent RLU value of the DOR-eGFP band in WT-vehicle animals. (**C**) Left: Representative Western blots to detect GPRASP1 protein or actine from 50 µg spinal cord lysates (each lane represents one mouse) or to detect GFP signal from immunoprecipitated DOR-eGFP using 0.5 mg of proteins from one mouse spinal cord followed by Western blots with anti-GFP-HRP antibodies. Right: Quantification of the GFP signal as % of the mean relative luminescent RLU value of the DOR-eGFP band in WT-vehicle animals. Data are represented as individual values and means ±SEM of n = 5–7 WT mice; n = 4–7 GPRASP1 KO mice. Statistical analysis by One way ANOVA followed by Tukey's post hoc test, * $P < 0.05$, ** $P < 0.005$; *** $P < 0.0005$.

non-fat dry milk (w/vol) for one hour before incubating with a primary antibody. Primary antibodies were incubated 2–3 h at room temperature (anti-GFP-HRP, anti-actine) or ON at 4°C (anti-GPRASP, anti-phospho DOR) with shaking. If required, after 2 quick and 5 long (5–5–15–5–5 min) washes, the relevant secondary antibody coupled with horse radish peroxidase was incubated (1 h at RT). Primary and secondary antibodies were diluted and incubated as described in Supp. Table S1. Chemiluminescence was used to reveal signal, by Immobilon^{R} Western (Chemiluminescent HRP substrate, P90720 WBKLS0500, Merk Millipore, Burlington, Vermont, USA) on a luminescent image analyzer (Amersham Imager 680, GE Healthcare Bio-science AB, Uppsala, Sweden) and protein expression was quantified by ImageQuant ™ TL software. If another antibody was used on the same membrane, desorption of the previous antibodies was performed with tris-glycine solution

(0.2 M HCl, 0.4 M Glycine in PBS pH7,4) before probing. Animals were males, homozygotes for DOR-eGFP (Fig. S4C, *D*), a mix of heterozygotes and homozygotes for DOR-eGFP (Fig. 2B, *C*, right panels). When a combination of heterozygotes and homozygotes for DOR-eGFP animals were used, DOR quantities were normalized to vehicle-treated GPRASP1 WT mice of the same genotype.

2.11. Immunohistochemistry

Brain sections were cut at 25 μm with a cryostat (Leica CM3050S) and stuck on slice (super frost plus Epredia J1800AMNZ) at room temperature prior storing at −20°C. Immunohistochemistry experiments were performed as described [44 and Supplementary data and methods]. Animals were males, homozygotes for DOR-eGFP.

2.12. Images acquisitions and analysis

Global slides acquisition was performed as described [56], with the slide scanner Nanozoomer 2 HT and fluorescence module L11600–21 (Hamamatsu Photonics, Japan, see Supplementary data and methods). Global DOR-eGFP positive neurons mainly from hippocampus, striatum, cortex and septum were detected from Nanozoomer files with NDPview software. Cellular distribution of DOR-eGFP signal was quantified from confocal images on Icy software using a macro [57]. Green-positive cells were selected (GFP signal+ AlexaFluor488) and manually delimited. The green fluorescence intensities were measured for the total cell area and for the subplasmalemmal area (4 pixels wide). The percentage of DOR-GFP in the subplasmalemmal area was then obtained by (multiplying the mean fluorescence intensity of GFP in the subplasmalemmal area by its area) divided by (the total area of the cell multiplied by its mean fluorescence intensity).

2.13. Co-immunoprecipitations of DOR-eGFP complexes from brain extracts

Brains were collected from groups with no CFA-inflammation, CFA-inflammation and CFA-inflammation + SNC80 treatment (n = 3 per groups). A non-fluorescent DOR-WT group was used as negative control. First, CFA (20 μl, s.c.) was injected to induce inflammation and SNC80 (10 mg/kg, i.p.) was administered three days later. Mice were sacrificed 15 min, 30 min, 2 h, 4 h and 24 h after SNC80 injection. In a last group of animals, a second administration of SNC80 was performed 24 h after the first one and organs were collected 30 min later. Brains were immediately frozen on dry ice and stored at −80°C. All the procedure was performed at 4°C and samples kept on ice as much as possible. In a 5 mL tube, one frozen brain was placed with 20 ceramic beads (1,4 mm in diameter) in 3 mL of lysis buffer (20 mM HEPES pH7,8, 50 mM NaCl, 0,5 % n-Dodecyl β-D-Maltopyranoside (DDM), 0,3 % 3-[(3-cholamidopropyl)diméthylammonio]-1-propanesulfonate (CHAPS), 7,5 mM iodoacétamide, cOmplete™ protease inhibitor cocktail 1x (11873580001, Roche, Darmstadt, Germany), phosphatase inhibitor (PhosSTOP 4906837001, Sigma-aldrich, France). 2 cycles of 15 sec at 4260 rpm with a 5 sec interruption in between were performed on bioprep-24R at 4°C (Allsheng). Samples were than centrifuged at 12 000 g for 10 min at 4°C to eliminate foam before collecting the supernatant. 3 mL of ice-cold lysis buffer were then added to the pellet before a novel cycle of homogenization at 4°C using the bioprep-24R. Supernatants were collected and incubated on a turning wheel at 4°C for 90 min. Debris not solubilized by lysis were then removed by centrifugation at 16 000 g 30 min at 4°C. A pre-clarification was realized on lysates with 40 μL of unloaded agarose beads (Bab-20 from Chromotek) on a turning wheel at 4°C for 30 min. Beads were removed by centrifugation for 5 min at 2500 g at 4°C, supernatants were collected and proteins were quantified by the Bradford method. 2.5 mg of brain proteins from one mouse were then mixed with 40 μl anti-GFP-Trap agarose beads (GTA-20, Chromotek) previously washed then conditioned with the lysis buffer. Co-immunoprecipitations using brain extracts from one mouse were performed in duplicates. DOR-eGFP immunoprecipitations were carried out for 16 h on a turning wheel at 4°C. On the following day, the supernatant was collected after centrifugation at 5 min at 2500 g at 4°C. Three washes of 1 mL (ice-cold Wash buffer with the same composition than lysis buffer except inhibitors) were done prior to dissociate the immunoprecipitated material from the GFP-beads in elution buffer (50 mM Tris HCl 50 mM DTT 1 % SDS 1 mM EDTA, 0,005 % bromophenol blue, 10 % glycerol) following twice the following procedure: 100 μl elution buffer, vortex for 15 min at RT, 95°C 5 min, centrifugation 16 000 g 5 min RT, 80 μl of supernatant collected for analysis. The two supernatants were pooled (160 μl in total) than stored before analysis (one aliquot of 40 μl for Western blot (25 % of the Co-IP) and one aliquot with the remaining 120 μl for Mass spectrometry analysis). Animals were males, homozygotes for DOR-eGFP.

2.14. In vivo phosphorylation studies

The kinetic of phosphorylation of DOR was assessed by Western blot from samples processed for DOR-eGFP Co-IP experiments from brain extracts using 12,5 % of the material for each blot. Phosphorylations of Threonine 361 and Serine 363 were revealed with corresponding antibodies according to [58,59] (Supp. Table S1) on two separate membranes resulting from the samples of the duplicated co-IP. The membranes were then desorbed to evaluate the total DOR-eGFP quantities with anti-GFP-HRP antibodies.

2.15. Mass spectrometry (AP-MS) analysis of the interactome of DOR-eGFP

The remaining of the DOR-eGFP co-immunoprecipitated material of one of the duplicates (n = 3 per groups) were reduced (dithiothreitol, 10 mM, 20 min at 25°C) and alkylated (iodoacetamide 50 mM, 30 min at 25°C) on cysteines, then co-affinity-precipitated proteins were resolved by SDS-PAGE and stained with colloidal Coomassie Blue (Euromedex, #10–0911) as previously described for the analysis of the interactome of metabotropic Glutamate 2 (GRM2) receptor from prefrontal cortex [60 and Supplementary data and methods). Briefly, as in [60], Protein Mass Spectra (MS) intensities were extracted as Label Free Quantification (LFQ) values from Maxquant protein groups results file considering only unique and razor peptides. Raw LFQ values were transformed into log base 2 values. Proteins matching reverse database or contaminants database were filtered out. An absence of signal in the bait samples, corresponding to Missing Not At Random (MNAR) values was interpreted primarily as absence of a stable or detectable interaction with the DOR-eGFP bait under the specific experimental conditions. Proteins were retained only if they had at least two measured MS intensities out of three replicates in at least one bait condition (i.e. at most one missing value out of three replicates in that condition) with the exception of proteins from the negative control immunoprecipitation, where proteins were retained regardless of the number of missing values so as not to exclude proteins that were not detected at all under the negative control conditions (potentially the best candidates for an interaction with DOR). For Figs. 5*A* and 5*B*, values were normalized on the most frequent values of protein LFQ observed in each MS injection [as in 60]. The list of proteins (Supp. Table S2) consists of those exhibiting a significant enrichment in co-immunoprecipitates, comparing protein LFQ in the negative control group with protein LFQ in each of the other group (Student Ttest, p-value < 0.05 [as in 60]). For Fig. 5*C* to Fig. 5*K*, Fig. 6 and Supp. Fig. S6, raw LFQ values were normalized to the LFQ values of DOR observed in each MS injection. Statistics were performed using Perseus software (v2.0.7.0) with two methods of implementation for the residual missing values. For Figs. 5*A* and 5*B* and Supp. Table S2 [as in 60], the "left-shifted normal distribution" approach implemented in the Perseus software for label-free proteomics data, with a down-shift of 1.8 and a width of 0.3 on the

log-intensity scale was used to replace missing values in each condition. This method assumes that missing values in IP-based LFQ datasets predominantly arise from undetected features and therefore replaces them with small random values sampled from a distribution modeled on the lower tail of the intensity distribution. Residual missing values were implemented to 0 for Fig. 5*C* to Fig. 5*K*, Fig. 6 and Supp. Fig. S6.

3. Results

Before addressing the role of GPRASP1 in the development of antinociceptive tolerance, we first verified that GPRASP1 interacts with DOR *in vivo* using DOR-eGFP mice. Indeed, when DOR-eGFP was immunoprecipitated from brain extracts using GFP-Trap beads, GPRASP1 was co-immunoprecipitated, as detected by Western blot with validated anti-GPRASP antibodies [61] (Supp. Fig. S1). As DOR-eGFP mice were previously demonstrated to show no detectable alteration in pain behavioral analyses neither in antinociceptive tolerance to DOR agonists as compared to wild-type mice [13,14,42,43], we then crossed this mouse line with GPRASP1 KO animals [36] and used the resulting DOR-eGFP/GPRASP1 KO mice in the rest of our study, unless otherwise stated.

3.1. Absence of antinociceptive tolerance to SNC80 in GPRASP1 KO mice

3.1.1. Neuropathic pain model

We first studied the role of GPRASP1 in the development of antinociceptive tolerance to the DOR agonist SNC80 in the chronic constriction injury (CCI) model. The anti-allodynic effect of SNC80 was evaluated daily in both males and females using the von Frey (VF) test. The basal mechanical sensitivities of the paw to calibrated filaments were 1.9 ± 0.1 g in WT males similar to 1.8 ± 0.1 g in GPRASP1 KO males (Figs. 1*A*) and 1.6 ± 0.1 g in WT females similar to 1.7 ± 0.1 g in GPRASP1 KO females (Fig. 1*B*). Nineteen days after surgery, allodynia (AD) was significantly observed in both genotypes and both sexes, the basal sensitivities of the paw being decreased to 0.3 ± 0.1 g in WT males and 0.4 ± 0.1 g in GPRASP1 KO males (Fig. 1*A*) and 0.4 ± 0.1 g in WT females similar to 0.5 ± 0.1 g in GPRASP1 KO females (Fig. 1*B*). Animals were then administered once a day with SNC80 (10 mg/kg, i.p., 45 min before testing). The anti-allodynic effect of the first administration of SNC80 on day 1 was similar in WT and GPRASP1 KO mice both in males and females (mechanical sensitivities back to 1.7 ± 0.2 g in WT males, 1.8 ± 0.2 g in GPRASP1 KO males, 1.7 ± 0.2 g in WT females and 1.9 ± 0.1 g in GPRASP1 KO females, with $p < 0.0001$ compared to vehicle treated groups, except for WT females with $p = 0.001$; $F = 93.58$ in males and $F = 24.4$ in females). In WT mice, the anti-allodynic action of SNC80 started to decline after the second administration and was completely absent from day 3 onwards both in males (Fig. 1*A*) and females (Fig. 1*B*), indicating the development of antinociceptive tolerance. In contrast, the anti-allodynic effect of SNC80 remained unaffected in GPRASP1 KO mice throughout the experiment (Fig. 1*A-B*). In the same cohorts, once tolerance to SNC80 was clearly established in WT mice, cold allodynia was assessed once using the cold plate (CP) test (Supp. Fig. S2). In WT males, the number of paw lifts was similar in vehicle and SNC80-treated groups showing tolerance to SNC80 in this thermal modality while in GPRASP1 KO males treated with SNC80, the number of paw lifts was significantly reduced compared to vehicle treated mice (10 ± 2 in WT + SNC80 compared to 3 ± 1 in GPRASP1 KO mice, $p < 0.05$, $F = 6.85$, Supp. Fig. S2A), indicating again that tolerance to SNC80 did not develop in GPRASP1 KO mice. SNC80-treated GPRASP1 KO females also display a diminished number of paw lifts as compared to SNC80-treated WT but not significantly (7 ± 2 in WT + SNC80 compared to 2 ± 1 in GPRASP1 KO mice, $F = 2.38$, Supp. Fig. S2B). Altogether, these results indicate that GPRASP1 is mandatory for the development of antinociceptive tolerance to DOR agonist SNC80 both in males and females exhibiting neuropathic pain.

3.1.2. Inflammatory pain model

We further investigated tolerance to SNC80 in male mice injected with Complete Freund Adjuvant (CFA, 20 µl, s.c.) at the base of the tail. To accelerate the development of antinociceptive tolerance, two consecutive administrations of SNC80 at 4 h intervals were performed on day 1 as in [13]. Thereafter, SNC80 was administered once a day for a total of 5 injections in 4 days (Fig. 1*C*). Note that for subsequent biochemical analyses of the same cohort, the brain and the lumbar spinal cord of these animals were collected at the end of the behavioral tests, when the antinociceptive effect of SNC80 was over (5 h after the fifth administration of SNC80).

Sensitivity of the animals to mechanical and thermal stimuli was assessed in the tail pressure (TPT) and tail immersion (TIT) tests, respectively, 45 min after each SNC80 injection (Fig. 1*C*). In the mechanical modality, basal nociceptive threshold and CFA-induced hyperalgesia (HA, measured 3 days after its injection) were similar in both WT and GPRASP1 KO mice (basal sensitivities to 186 ± 3 g in WT males similar to 196 ± 3 g in GPRASP1 KO males, dropping significantly to 122 ± 3 g in WT males similar to 127 ± 3 g in GPRASP1 KO males upon HA Fig. 1*C*). The first SNC80 administration (10 mg/kg) induced similar anti-hyperalgesic effects in WT and in GPRASP1 KO mice (back to 185 ± 6 g in WT males similar to 198 ± 6 g in GPRASP1 KO males, significantly different from the corresponding vehicle treated groups with $p = 0.0005$ for WT and $p < 0.0001$ for GPRASP1 KO mice, $F = 27.84$). In WT, this anti-hyperalgesic activity started to decline after the second administration of SNC80 and was completely absent at the third administration onward whereas SNC80 effect remained statistically significant in GPRASP1 KO mice at each injection ($p < 0.0001$ between vehicle and SNC80, $F = 27.84$). When measuring the thermal nociceptive threshold of the animals (Fig. 1*D*), again, while the SNC80 anti-hyperalgesic effect was significant in WT and GPRASP1 KO mice at the first injection compared to vehicle treated mice (6.8 ± 0.5 sec for vehicle treated and 9.4 ± 0.4 sec in SNC80 treated WT mice, $p = 0.0001$ between vehicle and SNC80; 5.7 ± 0.3 sec for vehicle treated and 9.6 ± 0.4 sec in SNC80 treated GPRASP1 KO mice, $p < 0.0001$); the fifth SNC80 anti-hyperalgesic effect remained statistically significant from vehicle treated animals only in GPRASP1 KO mice (5.9 ± 0.4 sec for vehicle treated and 7.6 ± 0.4 sec in SNC80 treated GPRASP1 KO mice, $p = 0.02$ between vehicle and SNC80, $F = 11.73$).

We next performed several control experiments. First, DOR selective antagonist naltrindole administration, 20 min before the fifth SNC80 administration (Nti, 5 mg/kg, s.c.), fully reversed the antinociceptive action of SNC80 in GPRASP1 KO mice in the mechanical modality, demonstrating that antinociception is mediated by the activation of DOR and not by an off-target action (Fig. 1*C* mechanical modality, dashed line 122 ± 7 g for the GPRASP1 KO Nti + SNC80 group instead of 167 ± 5 g for the GPRASP1 KO + SNC80 group, $p = 0.0004$). In the thermal modality, the Nti effect did not reach significance (Fig. 1*D* thermal modality, dashed histogram, 6.5 ± 0.6 sec for the GPRASP1 KO Nti + SNC80 group and 7.6 ± 0.4 sec for the GPRASP1 KO + SNC80 group, $p = 0.60$). Second, as previously reported [14], we confirmed that the acute anti-hyperalgesic effect and development of antinociceptive tolerance induced by repeated administrations of SNC80 were similar in DOR-eGFP and non-fluorescent DOR WT mice illustrating that the eGFP does not affect DOR function (Supp. Fig S3A-*B* mechanical modality S3*D-E* thermal modality). Then, we showed that antinociceptive tolerance to SNC80 was also absent in non-fluorescent DOR GPRASP1 KO mice (Supp. Fig. S3C-S3F). Finally, we investigated the consequences of repeated administrations of lower and higher doses of SNC80 (5 mg/kg and 20 mg/kg, respectively) in WT and GPRASP1 KO. The first injection of 5 mg/kg and 20 mg/kg of SNC80 produced anti-hyperalgesic effects in the mechanical modality in WT and GPRASP1 KO mice (Figs. 1*E* and 1*F*, $p = 0.02$ and $p < 0.0001$ compared to vehicle treated mice at the 20 mg/kg doses of SNC80 respectively). After the fifth SNC80 injection (5 mg/kg and 20 mg/kg), a significant anti-hyperalgesic response was still observed in GPRASP1 KO mice (Fig. 1*F*, $p = 0.03$ and $p < 0.0001$

compared to vehicle treated GPRASP1 KO mice at the 5 mg/kg and 20 mg/kg doses of SNC80 respectively) but not in WT mice (Fig. 1*E*). Likewise, an anti-hyperalgesic response to a fifth SNC80 injection was detectable in the thermal modality in GPRASP1 KO mice (Supp. Fig. S3G-*H* respectively, $p < 0.005$, SNC80 GPRASP1 KO compared to vehicle treated GPRASP1 KO mice).

Collectively, these results show that GPRASP1 is essential for the development of antinociceptive tolerance to SNC80 in two different models of persistent pain. Of note, also we did not score it, both WT and GPRASP1-KO mice displayed convulsive-like effects [21,51,62] upon injection of the first dose of 20 mg/kg of SNC80, but this effect disappeared after subsequent injections as reported previously for WT mice [21]. This suggests that GPRASP1 is not implicated in seizure tolerance.

3.2. SNC80-induced down-regulation of DOR-eGFP is similar in WT and GPRASP1 KO mice

We then investigated the consequences of the absence of GPRASP1 on the down-regulation of DOR elicited by a repeated SNC80 treatment *in vivo* using brain and spinal cord collected following the inflammatory pain experiment. ^{3}H-Deltorphine II saturation curves were established on brain membranes after the fifth administration of SNC80 (10 mg/kg) or of vehicle (Fig. 2*A*). In vehicle-treated animals, the K_D and Bmax values for DOR-eGFP were similar in WT and GPRASP1 KO mice (WT-vehicle, K_D: 2.7 ± 0.89; Bmax 100 ± 17 %; GPRASP1 KO-vehicle, K_D: 4.2 ± 1.33; Bmax 120 ± 13 % of WT-vehicle) suggesting that GPRASP1 does not significantly affect the total amount of DOR-eGFP nor its conformational states. As previously described [14], in DOR-eGFP mice, the receptor was massively degraded after the repeated treatment with SNC80 (81 ± 6 % of DOR receptor binding loss in WT + SNC80 compared to vehicle $p = 0.0016$, $F = 15.09$ Fig. 2*A*). Surprisingly, the same extent of down-regulation of DOR-eGFP was measured after the repeated SNC80 treatment of GPRASP1 KO mice (86 ± 3 % of DOR receptor binding loss in GPRASP1 KO + SNC80 mice compared to vehicle $p = 0.0006$, Fig. 2*A*). As a control showing that the eGFP tag does not affect DOR down-regulation, quantification of non-fluorescent DOR with ^{3}H-Deltorphine II in brain membranes of WT and GPRASP1 KO mice (Supp Fig. S4A) showed that repeated administrations of SNC80 (10 mg/kg, 5 times) induced the same level of non-fluorescent DOR reduction in presence or absence of GPRASP1. Moreover, quantification of DOR-eGFP with ^{3}H-Deltorphine II in mice treated with the lowest dose of SNC80 (5 mg/kg, 5 times) indicated less DOR reduction but to the same extent in GPRASP1 KO than in WT (57 ± 10 % of DOR receptor binding loss in WT + SNC80 and 54 ± 2 % in GPRASP1 KO + SNC80 compared to vehicle-treated animals; Supp. Fig. S4B). A high level of DOR down-regulation was observed following repeated administrations of the highest dose of SNC80 (20 mg/kg, 5 times) both in WT and GPRASP1 KO mice (83 ± 1 % of DOR receptor binding loss in WT + SNC80 and 88 ± 3 % in GPRASP1 KO + SNC80 compared to vehicle-treated animals, Supp. Fig. S4B).

We also quantified DOR-eGFP from the same brain membrane lysates by Western blot with anti-GFP antibodies in order to avoid any bias associated with radioligand binding experiments. As shown on Fig. 2*B*, the initial level of DOR-eGFP was similar in the presence or absence of GPRASP1 (WT-vehicle 100 ± 6 %; GPRASP1 KO-vehicle 98 ± 6 % of WT-vehicle) and the decrease in DOR-eGFP following SNC80 treatments (10 mg/kg, 5 times) was similar in WT and GPRASP1 KO mice (61 ± 3 % of GFP signal loss in WT + SNC80 and 67 ± 3 % in GPRASP1 KO + SNC80 compared to vehicle-treated animals, $p = 0.006$ and $p = 0.004$ respectively, $F = 10.11$). DOR down-regulation quantified by WB also showed a dose/effect with SNC80 (47 ± 9 % of DOR receptor binding loss in WT + 5 mg/kg SNC80 and 65 ± 14 % in GPRASP1 KO + 5 mg/kg SNC80 compared to vehicle-treated animals; 69 ± 8 % of DOR receptor binding loss in WT + 20 mg/kg SNC80 and 80 ± 3 % in GPRASP1 KO + 20 mg/kg SNC80 compared to vehicle-treated animals, Supp. Fig. S4C-*D*).

We next immunoprecipitated DOR-eGFP from lumbar spinal cord extracts with anti-GFP-trap beads and quantified the receptor by Western blotting with anti-GFP antibodies (Fig. 2*C*). The level of DOR was similar in vehicle-treated WT (100 ± 5 % of GFP signal) and GPRASP1 KO mice (91 ± 17 % of GFP signal of WT-vehicle). The down-regulation of spinal DOR was similar to that measured in the brain (10 mg/kg, 5 times) in both WT and GPRASP1 KO mice (65 ± 4 % of DOR receptor binding loss in WT + SNC80 and 69 ± 4 % in GPRASP1 KO + SNC80 compared to vehicle-treated animals, $p = 0.0003$ and $p = 0.0006$ respectively, $F = 14.80$), indicating that DOR down-regulation also takes place in the spinal cord where it is not affected by the absence of GPRASP1. Taken together, these results show that GPRASP1 is not necessary for DOR down-regulation elicited by a repeated SNC80 administration.

Since GPRASP1 is implicated in the development of antinociceptive tolerance to DOR agonist but not in DOR down-regulation, we analyzed further, using the inflammatory pain model, potential differences in the cellular and molecular environment of DOR-eGFP between WT and GPRASP1 KO mice that could explain the mechanism of antinociceptive tolerance mediated by GPRASP1.

3.3. GPRASP1 is involved in the dynamic of DOR at the plasma membrane in response to inflammation and SCN80 treatment

We first investigated whether the absence of GPRASP1 had any effect on the subcellular localization of DOR-eGFP. Brains from saline mice and CFA-inflamed mice, repeatedly treated or not with SNC80, were collected 24 h after the 5th administration of SNC80 and DOR-eGFP subcellular distribution was analyzed in the brain by confocal microscopy. As previously described [13,14,42–45], the DOR-eGFP signal was at the plasma membrane with detectable signal within cytoplasmic organelles (Fig. 3*A*).

As shown in Fig. 3*B*, analysis of the percentage of DOR-eGFP fluorescence at the plasma membrane vs fluorescence of the entire cell indicated that neurons from CFA-treated WT mice had a significantly higher number of receptors localized at or close to the plasma membrane as compared to saline-treated mice (32.72 ± 0.87 % after CFA compared with 26.47 ± 1.17 % before CFA, $p < 0.0001$, $F = 11.02$). Conversely, no difference was observed between saline- and CFA-GPRASP1 KO mice (26.76 ± 0.89 % after CFA compared with 29.86 ± 0.77 % before CFA). Twenty-four hours after the 5th SNC80 injection, the proportion of DOR-eGFP at the plasma membrane was significantly reduced in WT mice (24.67 ± 1.11 % in CFA + SNC80), as compared to vehicle-treated CFA-mice ($p < 0.0001$), suggesting a shift in the distribution of the subcellular localization of the remaining DOR towards intracellular organelles. Again, no difference was observed in GPRASP1 KO mice between vehicle- and SNC80-treated CFA-mice (26.26 ± 0.80 % in CFA + SNC80). Altogether, these results indicate that GPRASP1 might play a role in the dynamic of DOR subcellular localization in response to inflammatory and SNC80 stimuli.

3.4. Phosphorylation of DOR-eGFP is similar between WT and GPRASP1 KO mice

Desensitization and β-arrestin-dependent internalization of DOR have been proposed to depend upon phosphorylation on two residues of DOR C-tail, Threonine (T361) and Serine (S363) [58,59]. We therefore examined kinetics of these phosphorylation sites on immunoprecipitated DOR-eGFP from brain extracts using GFP-Trap beads after one or two administrations of SNC80 (on day 1 and day 2) in CFA-inflamed mice (Fig. 4*A*). In WT mice, S363 phosphorylation of DOR peaked at 15 min after SNC80 administration as compared to non-activated mice and then decreased to return to basal level 24 h after SNC80 injection on day 1 (Fig. 4*A-B*). After a second SNC80 stimulation of 30 min on day 2, S363 phosphorylation was similar to that of the first stimulation. S363 phosphorylation was modulated by SNC80 in GPRASP1 KO mice with

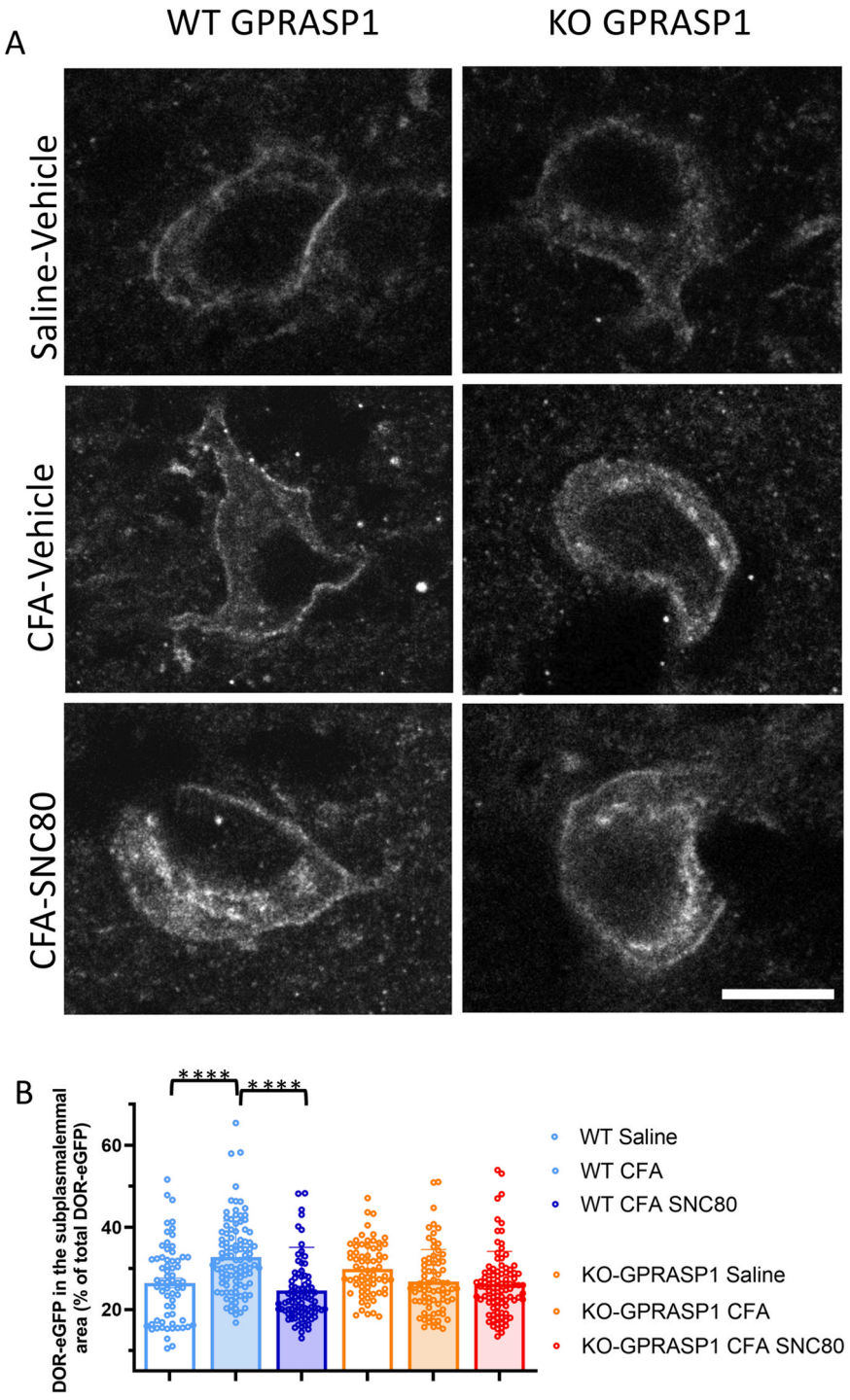

Fig. 3. Dynamic of DOR-eGFP localization at the plasma membrane is different in brains of DOR-eGFP/GPRASP1-WT versus DOR-eGFP/GPRASP1 KO mice. (**A**) Representative confocal images of DOR subcellular localization assessed by immunofluorescence of DOR (GFP revealed by signals from direct GFP-fluorescence together with anti-GFP/ alexafluor 488) in brain slices of vehicle- and SNC80-treated WT and GPRASP1 KO mice. Brains were dissected out 24 h after the fifth SNC80 administration. Scale bar 8 μm. (**B**) Proportion of DOR-eGFP in the sub-plasmalemmal compartment in percent of the whole fluorescence signal of the cell. Briefly, the green fluorescence intensities were measured for the total cell area and for the subplasmalemmal area (4 pixels wide). The percentage of DOR-GFP in the sub-plasmalemmal area was then obtained by (multiplying the mean fluorescence intensity of GFP in the subplasmalemmal area by its area) divided by (the total area of the cell multiplied by its mean fluorescence intensity). Data are represented as individual values and means ± SEM of n = 65 neurons WT saline, n = 103 WT-CFA, n = 86 WT-CFA+SNC80, n = 69 neurons GPRASP1 KO saline, n = 77 GPRASP1 KO-CFA, n = 96 GPRASP1 KO-CFA+SNC80 counted in each group with 4 mice/ group. Statistical analysis by One-way ANOVA analysis followed by Tukey's post hoc test, **** $P < 0.0001$.

similar amplitude and kinetics. We made the same observation for the phosphorylation of DOR on T361, which reached a maximal level 2 h after the first SNC80 administration on day 1 and remained at a high level 4 h after, both in WT and GPRASP1 KO mice (Figs. 4*A* and 4*C*). Following the second SNC80 injection of 30 min on day 2, the phosphorylation of T361 was similar to that measured after the first injection in WT and GPRASP1 KO mice. Collectively, these results suggest that desensitization kinetic to SNC80, as measured by phosphorylation of

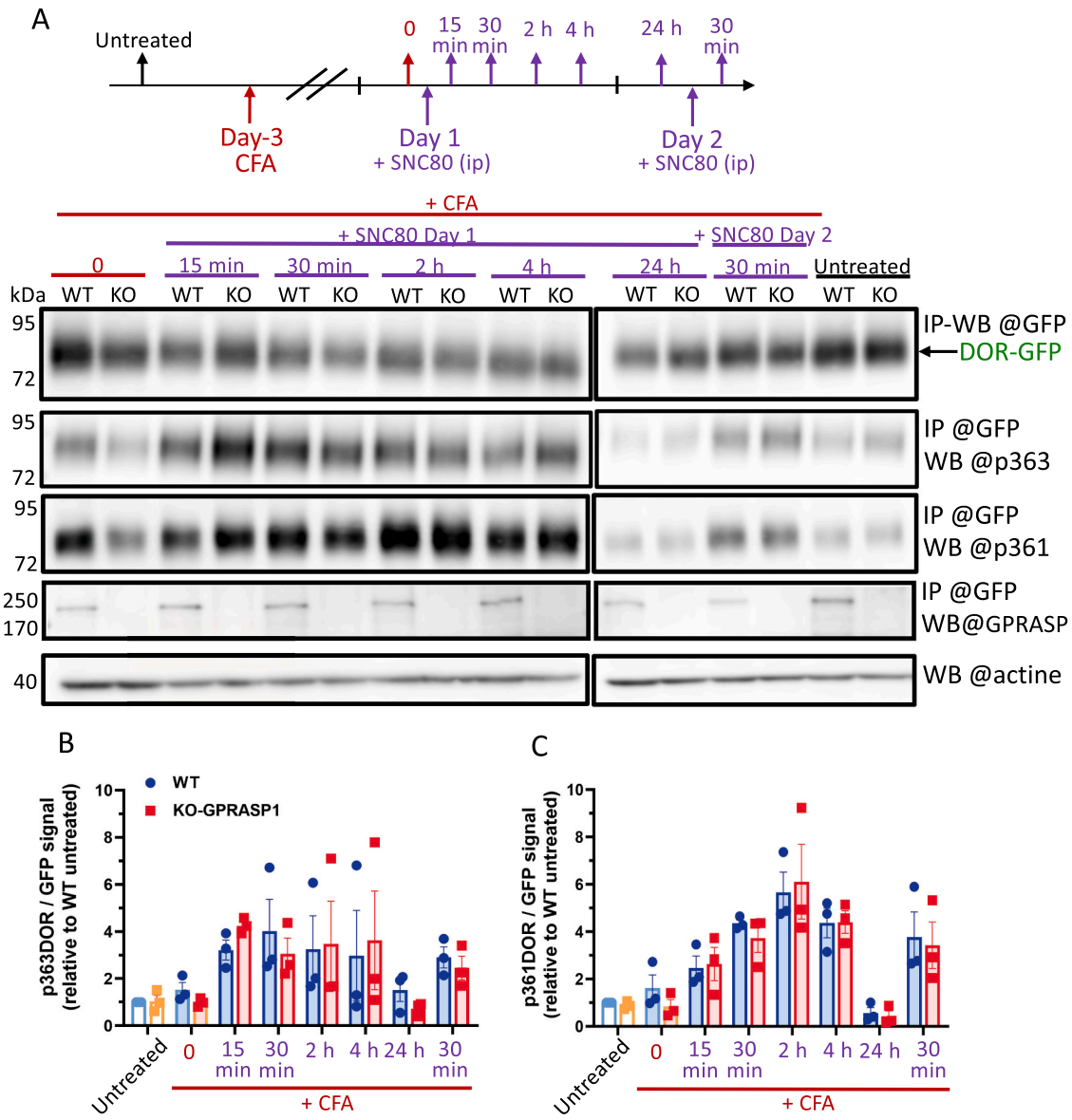

Fig. 4. DOR phosphorylation as a function of time after SNC80 activation is similar in brain of DOR-eGFP/GPRASP1-WT versus DOR-eGFP/GPRASP1 KO mice. Phosphorylations of DOR-eGFP was evaluated in untreated condition, CFA-inflamed conditions and following one or two stimulations by SNC80 at 24 h intervals (10 mg/kg, i.p.). DOR-eGFP was immunoprecipitated (IP) on anti-GFP-trap beads from brain extracts of homozygotes DOR-eGFP male mice in duplicates and the immunoprecipitated material was analyzed by Western blot. (**A**) Scheme of the 8 time-points of brain dissections before and after SNC80 injections. Representative Western blots used to quantify DOR phosphorylations, to detect total DOR-eGFP, actine and GPRASP1. (**B, C**) Quantifications of phosphorylations of DOR-eGFP on Serine 363 (B) and on Threonine 361 (C) normalized to the DOR-eGFP signal detected on the same Western blot membrane. Data are represented as individual values and means ± SEM of n = 3 male mice/time-point/genotype. Untreated conditions (light blue=WT, orange= GPRASP1 KO), CFA SNC80 WT mice in dark blue, CFA SNC80 GPRASP1 KO mice in red.

DOR-eGFP, are similar between WT and GPRASP1 KO mice. Of note, in this experiment, GPRASP1 co-immunoprecipitated with DOR-eGFP from brains of WT mice at all time points before and after SNC80 activation and not from control GPRASP1 KO animals (Fig. 4*A*). Surprisingly, no significant variation in the amount of GPRASP1 associated with DOR-eGFP could be observed during the time-course of SNC80 activation, suggesting that GPRASP1 interacts with DOR in a constitutive manner.

3.5. Coupling of DOR-eGFP with heterotrimeric Gi/o proteins is not affected by the absence of GPRASP1

We further analyzed putative difference in desensitization of DOR by measuring G protein coupling to DOR using an interactomic approach. The interactome of DOR-eGFP was compared in four conditions: untreated, CFA-inflamed mice before and 30 min after the first SNC80 injection when antinociception is present and after the second SNC80 injection when differences in antinociception between WT and GPRASP1 KO mice are developing. Proteins from brain lysates that co-immunoprecipitated with DOR-eGFP using GFP-Trap beads were identified by mass spectrometry MS and compared with a negative control using non-fluorescent DOR-WT brain lysates subjected to the same protocol with GFP-Trap agarose beads. Overall, 778 proteins out of 1386 detected proteins were significantly more abundant in one condition at least over the negative control ($P < 0,05$, Supp. Table S2). As expected, DOR and the eGFP were among the most enriched proteins in the immunoprecipitates as compared to negative controls, both in WT and GPRASP1 KO mice (see in Fig. 5*A-B* Volcano plots illustrating the

difference in protein abundance in DOR-GFP immunoprecipitates for each identified protein by MS from DOR-eGFP/GPRASP1-WT or GPRASP1 KO mice brain versus negative control CNTR immunoprecipitates, respectively). In WT CFA-inflamed mice, the first and second SNC80 administrations induced significant increases in Gα subunits of heterotrimeric $G_{i/o}$ proteins associated with DOR, compared to conditions without SNC80 (Gαi1, Gαi2, Gαi3, Gαo1 and Gβ1, Gβ2 in Fig. 5*C-H,* respectively, statistical analyses by volcanoplots comparing non-activated versus the second SNC80 injection in Supp. Fig. S5). Of note, the heterotrimeric Gγ subunits were not identified in the interactome of DOR. Likewise GPRASP1 was not detected by MS while it was detected in DOR-eGFP immunoprecipitates by Western blot (Fig. 4*A*) illustrating some limits in our AP-MS procedure. β-arrestin2 was not found either, while β-arrestin 1 (ARRB1) was present but not significantly enriched in any conditions of the DOR interactome (Fig. 5*A*, *B*, Supp. Table S2) suggesting that at the time-point 30 min after SNC80 activation, most activated DOR were still engaged in G-protein coupling. Gβ5 was present in the interactome but was not modulated by SNC80 (Fig. 5*I*), while surprisingly, Gαz was significantly enriched in the DOR interactome upon the second SNC80 activation over the non-activated DOR as well as Gαs, although in a non-significant manner (Fig. 5*J-K* and Supp. Fig. S5).

Overall, the interactome of DOR was almost identical between WT and GPRASP1 KO mice. Importantly, in the absence of GPRASP1, heterotrimeric $G_{i/o}$ proteins were also enriched in the DOR interactome after a first then a second SNC80 activation (Fig. 5*C-H* and for the statistical analyses presented by volcanoplots see Supp. Fig. S5) and their levels in the co-immunoprecipitates were not significantly different to that measured in WT mice. Taken together, these results indicate that GPRASP1 does not modulate DOR coupling to heterotrimeric G proteins in CFA-inflamed mice following one or two SNC80 administrations at 24 h intervals. In addition, the fact that we detected SNC80-induced coupling of different pools of DOR to different pools of $G_{i/o}$ proteins demonstrated the robustness of our quantitative biochemical approach to purify DOR interacting proteins.

3.6. Synaptic proteins identified in the DOR interactome

Several proteins known to be enriched in neurons and in synapses (pre and/or post-synaptic) were identified in the DOR interactome of untreated WT mice (Fig. 5*A* protein names labeled in black). One of the most abundant proteins compared to negative control was GP158 (Fig. 5*A*), an unconventional GPCR for glycine [63]. Several other GPCRs were enriched in the interactome of DOR such as the metabotropic glutamate receptors (GRM1 and GRM3) and the cannabinoid receptor (CNR1) as well as ionic channels (Fig. 5*A*). With scarce exceptions (protein names labeled in dark blue for WT mice, Fig. 5*A* or in dark red for GPRASP1 KO mice Fig. 5*B)*, there was no significant difference in the levels of these neuronal and synaptic proteins in DOR interactome between WT and GPRASP1 KO mice in any conditions (compare untreated WT mice, Fig. 5*A;* protein names labeled in black with untreated GPRASP1 KO mice Fig. 5*B;* protein names labeled in black and comparison of all 4 conditions before and after SNC80 activation in the two genotypes Supp. Fig. S6A-*L*). The excitatory amino-acid transporter 4 (EAA4) and the semaphorin 4 A (SEM4) became less associated with DOR after the second activation with SNC80 in WT mice and significantly less in GPRASP1 KO mice as compared to WT animals (Supp. Fig. S6E-*F,* respectively).

3.7. Differences in the DOR interactome between WT and GPRASP1 KO mice

A few proteins were in complex with DOR in a GPRASP1-dependent manner. In untreated animals, the signaling Receptor-type tyrosine-protein phosphatase epsilon (PTPRE) was significantly enriched with DOR compared to negative controls only in WT mice (compare protein name labeled in light blue Fig. 5*A* with Fig. 5*B* and Fig. 6*A*) while inversely the Dolichol-phosphate mannosyl-transferase subunit 1 (DPM1) was significantly more associated with DOR in the absence of GPRASP1 (compare Fig. 5*A* with protein name labeled in orange in Fig. 5*B* and Fig. 6*B*). The Synapse differentiation-inducing gene protein 1 (SYNG1 or SYNDIG1), an auxiliary subunit of glutamatergic ionotropic (AMPA) receptors [64], co-immunoprecipitated with DOR both in WT and GPRASP1 KO untreated mice (Fig. 5*A* and *B*). Unexpectedly, SYNG1 was very strongly recruited to SNC80 activated DOR in both genotypes (Fig. 6*C* and Supp Fig. S5). Compared to the first SNC80 activation, SYNG1 abundance was significantly higher after the second SNC80 activation on day 2 only in WT mice (Fig. 6*C*). Although not significant ($P = 0.068$), there was a difference of SYNG1 amount between the interactome of DOR-eGFP in WT and GPRASP1 KO after the second SNC80 injection. The response of SYNG1 to SNC80 was unique, since DOR association with another auxiliary subunit of AMPA receptors, the Proline-rich transmembrane protein (PRRT1 = SYNDIG4) or with the AMPA selective Glutamate receptor 2 (GluR-2 = Gria2) itself was not modulated upon DOR activation by SNC80 (Fig. 5*A-B*, Fig. 6*D-E* and Supp. Fig. S5).

A few proteins became associated with DOR upon the second SNC80 administration vs non-activated CFA-inflamed WT mice but not significantly associated to DOR in GPRASP1 KO mice (compare Supp. Fig. S5A-*B*): the Mitogen-activated protein kinase 1 (ERK-2 for Extracellular Regulated kinase 2, Fig. 6*F*), the Potassium-Channel Tetramerization Domain Containing 12 (KCTD12, Fig. 6*G*) and the Ubiquitin carboxyl-terminal hydrolase 5 (UBP5, for Ubiquitin-Binding Protein 5, Fig. 6*H*), contrary to ubiquitin that was significantly enriched after the second SNC80 injection in both WT and GPRASP1 KO mice (Fig. 6*I*). Both the membrane trafficking sorting nexin Rho GTPase-activating protein (peptides detected by MS corresponding either to RHG33 or RHG32) and the signaling C-Maf-Inducing protein (CMIP), became specifically recruited to twice activated DOR only in WT mice (identified in four replicates out of six SNC80 activated samples Fig. 6*J* and *K*), while in the absence of GPRASP1, it was the E3 ubiquitin-protein ligase (RNF126) that became instead recruited to SNC80 activated DOR (identified in four replicates out of six Fig. 6*L*).

Taken together, these results suggest that, already at steady state and further upon activation, GPRASP1 modulates the interaction of DOR with a subset of proteins, some of which could participate together with GPRASP1 in the development of antinociceptive tolerance.

4. Discussion and conclusion

4.1. Uncoupling antinociceptive tolerance from receptor down-regulation during repeated activation of DOR in persistent pain: mandatory role of GPRASP1

In this study, we demonstrate that SNC80 produces a persistent and complete anti-hyperalgesic effect in both male and female GPRASP1 KO mice in a neuropathic pain model as well as in male GPRASP1 KO mice in an inflammatory pain model, that did not lessen upon daily injections. Due to a combination of technical, ethical, and financial constraints, female mice were not tested in the inflammatory pain model. Nevertheless, we propose that GPRASP1 is required for the development of antinociceptive tolerance to SNC80, a high-internalizing DOR agonist [13,21,51] regardless of the pain model or the sex of the animals. Together with β-arrestin 1, GPRASP1 represents the second DOR-interacting protein reported to produce a clear phenotype of reduced antinociceptive tolerance to SNC80. β-arrestin 1 had previously been implicated in the development of analgesic tolerance to SNC80 using an inflammatory pain model similar to ours, except that complete Freund's adjuvant (CFA) was injected into the plantar surface of the hind paw in both male and female mice [20,21] rather than the base of the tail. In β-arrestin 1 KO mice, an anti-hyperalgesic effect was observed following each daily SNC80 injection; however, the effect was less robust than that observed in GPRASP1 KO mice. This difference may be

attributable to variation in SNC80 dosing, as the study using β-arrestin 1 KO mice reported increased SNC80 efficacy at the first injection compared to WT mice. To maintain equipotent conditions, the SNC80 dose used in WT mice was 10 mg/kg, whereas it was reduced to 3 mg/kg in β-arrestin 1 KO mice [21]. In our inflammatory pain model, we tested three SNC80 doses, and the results suggested that SNC80 was approximately equipotent in the two genotypes: GPRASP1 KO mice displayed significant anti-hyperalgesic responses to SNC80 at the first injection of 5, 10, or 20 mg/kg.

Previous cellular assays suggested that GPRASP1 promotes DOR degradation via lysosomal pathways [23,29]. To explore this *in vivo*, we compared DOR levels in WT and GPRASP1 KO inflamed male mice following a repeated SNC80 treatment using radioligand binding and DOR-eGFP Western blotting. Despite differences in methodology

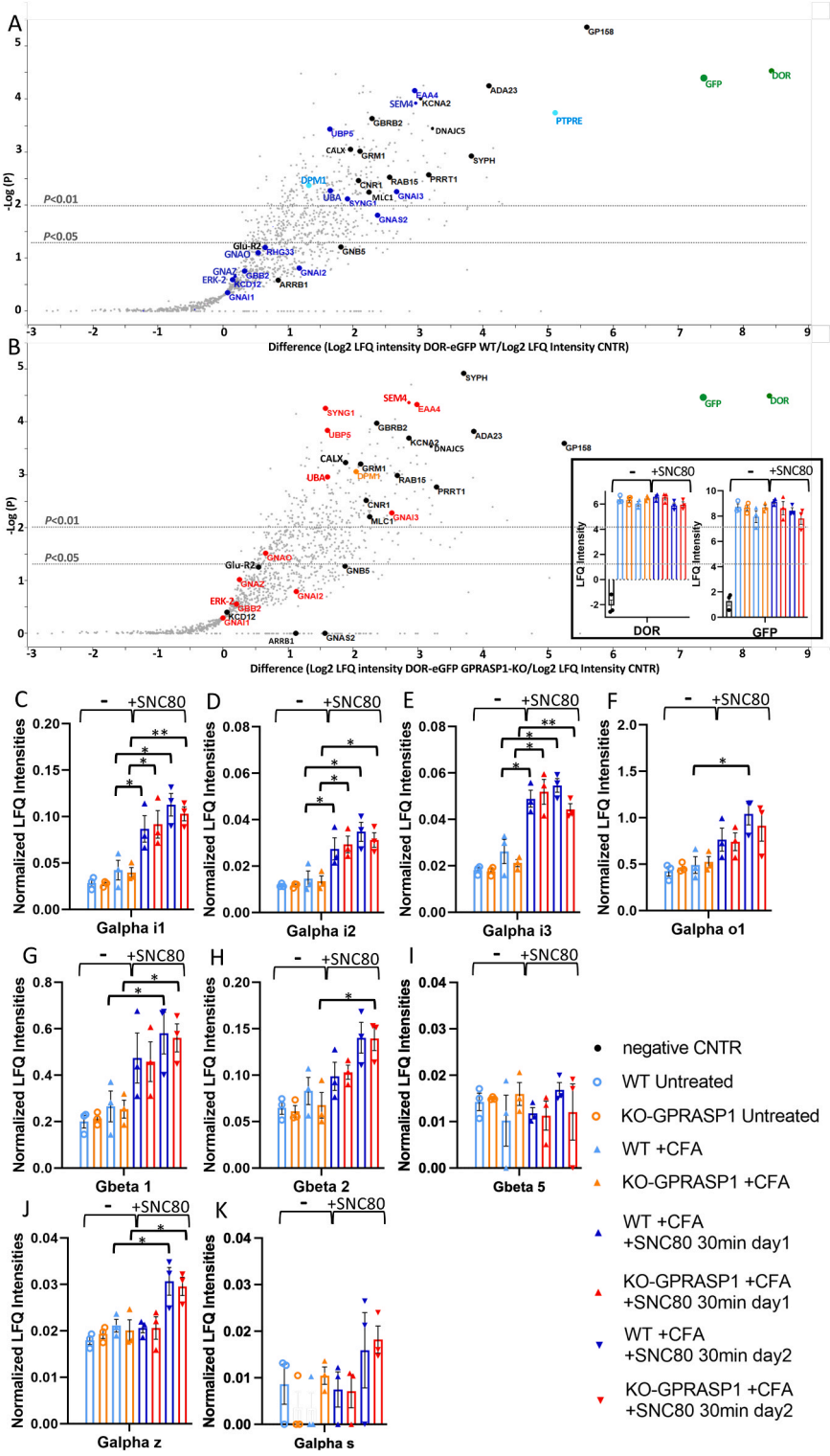

(caption on next page)

Fig. 5. DOR-eGFP coupling to Gi/o proteins is similar in brain of WT and GPRASP1 KO mice activated once or twice by SNC80. DOR-eGFP was immunoprecipitated on anti-GFP-trap beads from 2.5 mg of protein brain extracts/per mice and analyzed by mass spectrometry MS n = 3 male mice/time-point/genotype. (**A, B**) Volcano plot illustrating the difference in protein abundance in DOR-GFP immunoprecipitates for each identified protein by MS from DOR-eGFP/GPRASP1-WT untreated mice brain versus negative control CNTR immunoprecipitates (non-fluorescent DOR-WT/ GPRASP1-WT) (A) and from DOR-eGFP/GPRASP1 KO untreated mice brain versus negative control CNTR immunoprecipitates (B). Proteins with two or three missing values represented 6.68 % of proteins in the WT interactome and 9.38 % in the GPRASP1 KO interactome, indicating that the fraction of highly missing features used for interpretation is limited. Missing values were implemented randomly as part of a normal distribution (width 0.3, down shift 1.8) for statistical analysis using Perseus software with Student T test. DOR and GFP are labeled in green. Proteins that were modulated according to a treatment are labeled in dark blue (A) or red (B). Inset in (B): Comparison of DOR and GFP detected in the DOR-eGFP immunoprecipitated materials analyzed by MS between 4 conditions: untreated mice, CFA-inflamed, CFA-inflamed 30 min after a first SNC80 administration or 30 min after a second SNC80 administration at 24 h intervals). Protein MS intensities were extracted as Label Free Quantification (LFQ) values. Raw LFQ values were transformed into log base 2 values. Protein LFQ intensities in the negative control group are compared with protein LFQ intensities in each of the other groups. Data are represented as individual values and means ± SEM of n = 3 mice. (**C**, **D**, **E**, **F**, **G**, **H**, **I**, **J**, **K**): Comparison of raw LFQ intensities of each heterotrimeric G protein subunits detected in the DOR-eGFP immunoprecipitated material between the 4 conditions normalized to the raw LFQ value of DOR observed in each MS injection. Data are represented as individual values and means ± SEM of n = 3 mice. The missing values were implemented with a single value of 0 for statistical analysis using Perseus software with Student T test excluding conditions with 2 or 3 missing values (no histogram depicted). * $P < 0.05$, ** $P < 0.005$.

(radioligand binding using an agonist detecting mainly high-affinity receptors and Western blotting detecting total DOR) both approaches showed similar receptor degradation across genotypes. This indicates that GPRASP1 is not essential for DOR degradation *in vivo*. Using this time two methods, our findings are clearly confirming prior works showing that *in vivo*, degradations of cocaine-stimulated D2R or chronically activated β2-adrenoceptors are not dependent on the expression of GPRASP1 [36,40]. In addition, GPRASP1 was also shown in these previous studies to be necessary for the establishment of detrimental adaptations following repeated GPCR's activations, including tolerance in the case of activated β2-adrenoceptors, suggesting a common molecular mechanism, implicating GPRASP1, that is not related to receptor degradation [40].

Our results suggest as well that antinociceptive tolerance in WT mice does not result directly from DOR loss. Yet, pre-treatment with the highly selective DOR antagonist naltrindole abolished the sustained anti-hyperalgesic effect of SNC80 in GPRASP1 KO mice. From our Western blot experiments using brain or spinal cord extracts to quantify DOR, it appears that approximately 20 % of the remaining DOR receptors may be sufficient to elicit a complete antinociceptive effect of SNC80 in GPRASP1 KO mice. In our previous study involving chronic activation of β_2-adrenoceptors with formoterol, less than 40 % of the receptors remained in GPRASP1 KO mice following chronic exposure to the formoterol agonist [34]. Nevertheless, formoterol produced a full bronchodilatory effect in these mice, whereas it showed no effect in WT mice [34]. This raised the hypothesis that the remaining DOR in GPRASP1 KO mice retains full signaling capacity, while in WT mice, a similar residual pool of DOR may be desensitized or otherwise functionally impaired.

4.2. Coupling to heterotrimeric G protein is unaltered between WT and GPRASP1 KO mice

To address this, we evaluated DOR coupling to heterotrimeric G proteins. We first analyzed DOR phosphorylation, a hallmark of desensitization. *In vitro*, SNC80 induces rapid phosphorylation at Ser363 followed by Thr361 [59]. We assessed these phosphorylation events after two SNC80 injections spaced 24 h apart and found similar phosphorylation kinetics in WT and KO mice. We then analyzed DOR coupling to Gαi/o subunits using quantitative proteomics. We could detect the coupling of DOR upon SNC80 activation with all the Gαi/o subunits. No difference in coupling extent was observed between WT and GPRASP1 KO mice, suggesting intact G protein activation in both genotypes. Notably, while Ser363 phosphorylation has been linked to DOR internalization *in vitro*, a recent study questioned the requirement of phosphorylations in a presynaptic DOR overexpression neuronal model [65]. Our results support this ambiguity, as phosphorylation and G protein coupling kinetics overlapped, suggesting that phosphorylation of Ser363 may not drive desensitization of DOR *in vivo*.

4.3. Novel role of GPRASP1 in trafficking and signaling rather than degradation of DOR

Kinetics of the interactome of DOR upon activation with an agonist have already been studied *in vitro* [66,67]. The interactome of DOR using forebrain extracts of a knock-in flag-tagged-DOR mouse line has been characterized as well, but in naive animals only [68]. To investigate further how DOR could be functionally impaired upon repeated activations in mice expressing GPRASP1, we examined for the first time the DOR interactome in brain samples as a function of activation using four conditions: untreated mice, CFA-inflamed, or following one or two SNC80 treatments. First, the identification of all Gαi/o proteins with activated DOR represents a very strong and specific quality control of our DOR interactomic analysis. Second, using our AP-MS analysis of brain samples, with a different mouse line, and a different biochemical procedure, we confirm several DOR-associated proteins, including several GPCRs and membrane channels identified in the previous study [68] and their enrichment was constant across genotypes and conditions: GP158 [63] was the most enriched protein but also CNR1, GRM3, the β2 subunits of the GABA A chloride channel receptor GABRB2, the voltage-gated potassium channels (KCNA2 =Kv1.2) and EAA4. We also confirm RAB15, a small GTPase but not RAB10, while the latter was demonstrated to play a role in DOR exocytosis using HEK293 cell heterologous expression [68]. New interactors identified in our study included GRM1, astrocyte-associated membrane protein (MLC1), synaptophysin (SYPH), semaphorin (SEM4), and Disintegrin and metalloproteinase domain-containing protein 23 (ADA23). DnaJ homolog subfamily C member 5 (DNAJC5), a chaperone implicated in synaptic exocytosis [69], was also strongly enriched. As DOR is expressed in pre- and post-synaptic neurons as well as in astrocytes, our results indicate that we have immunoprecipitated different pools of DOR depending on its cellular expression. The constant presence of these proteins in complex with DOR across conditions and time of activation suggests that the majority of DOR remains at the plasma membrane or synaptic sites up to 30 min post-SNC80. However, EAA4 and SEM4 showed reduced association with DOR following the second SNC80 administrations, implying possible receptor relocalization upon repeated activations.

Among novel findings, SYNG1 emerged as a particularly interesting DOR interactor. SYNG1 has not been previously associated with any GPCR signaling [64], yet we observed its robust recruitment to DOR following SNC80 activation. The interaction seems unrelated to AMPA receptor activity, as neither AMPA receptors nor PRRT1 showed increased association with DOR. Other potential DOR signalosome components identified included ERK-2, KCTD12, and UBP5. Interestingly, KCTD12 has been linked to MOR desensitization [70], while UBP5 regulates Cav3.2 channel stability in pain pathways [71]. These proteins may thus contribute to DOR signaling and antinociceptive response.

Although the overall DOR interactome was similar between genotypes, we identified notable differences. In WT untreated mice, DOR

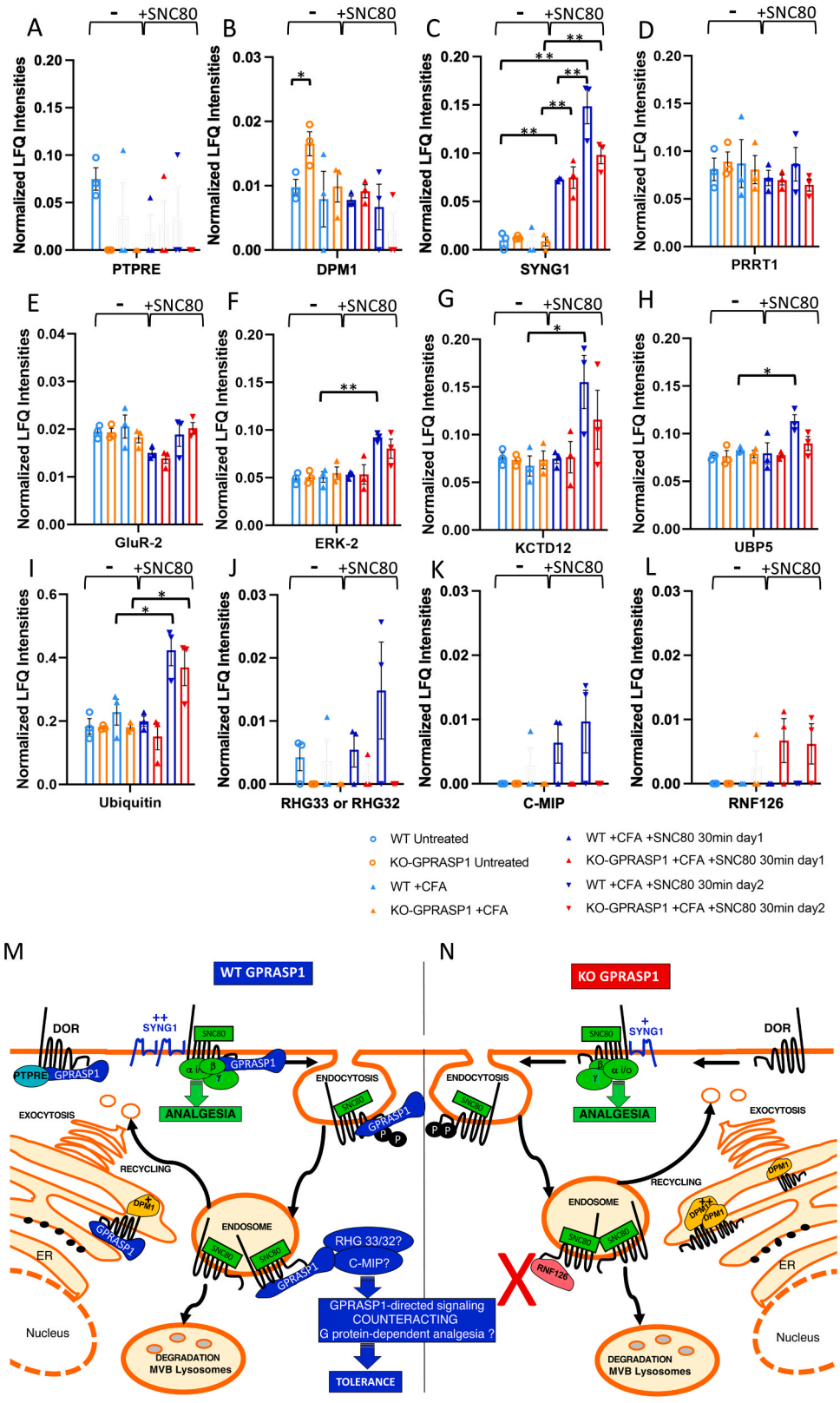

Fig. 6. Differences in DOR interactome between WT and GPRASP1 KO brains. (**A, B, C, D, E, F, G, H, I, J, K, L**) Comparison of raw LFQ intensities of each novel protein detected in the DOR-eGFP immunoprecipitated material between the 4 conditions normalized to the raw LFQ value of DOR observed in each MS injection. Data are represented as individual values and means ± SEM of n = 3 mice. The missing values were implemented with a single value of 0 for statistical analysis using Perseus software with Student T test excluding conditions with 2 or 3 missing values (no histogram depicted). * $P < 0.05$, ** $P < 0.005$. (**M, N**) Proposed model for the role of GPRASP1 and the newly identified proteins in complex with DOR in the development of antinociceptive tolerance to SNC80 agonist by the activation of signaling events counteracting G-protein dependent antinociception in WT mice (M) that are absent in GPRASP1 KO mice (N).

interacted selectively with the phosphatase PTPRE, which negatively modulates voltage-gated K^+ channels [72]. This interaction was absent in GPRASP1 KO mice and may influence receptor priming in inflammatory conditions [9,73]. However, this association diminished in inflamed WT mice, leaving its role in tolerance unclear. Conversely, in untreated GPRASP1 KO mice, DOR showed increased association with DPM1 and RNF126. DPM1 is involved in N-glycosylation in the endoplasmic reticulum (ER) [74] and interestingly, using the ligation proximity assay *in vitro*, a proximity of MOR with DPM1 was reduced upon MOR activation [70]. In addition, RNF126 was shown *in vitro* to regulate the sorting of the chemokine GPCR CXCR4 towards lysosomes [75]. These suggest prolonged ER residency together with an altered DOR trafficking in the absence of GPRASP1. Fluorescence microscopy on brain neurons confirmed subtle differences in intracellular trafficking of DOR between genotypes. On the other hand, differences in receptor localization may not fully explain tolerance since SNC80 can penetrate inside cells due to its hydrophobicity where it stabilizes DOR in its active form [76], and since endosomal DOR signaling contributes to antinociception [77].

Our working hypothesis is that GPRASP1 may participate in a negative-feedback signaling mechanism that limits antinociceptive signaling, thereby contributing to tolerance. (Fig. 6*M, N*). A role of GPRASP1 in signaling is supported by *in vitro* studies indicating that GPRASP1 expression can modulate GPCR signaling such as Gq-, Gs-, MAPkinase pathways, and NFKB- or CREB-dependent transcriptional signaling in the case of the viral chemokine receptor US28, of insulin secretion of the glucagon-like peptide GLP-1 receptor or of β2-adrenoceptors [40,78,79]. Our proposed negative-feedback model is further supported by our recent study in mice, which demonstrated that GPRASP1 is required for the development of both tolerance and the paradoxical bronchial hyperreactivity induced by chronic activation of β_2-adrenoceptors with formoterol [40]. Indeed, how else can the simultaneous occurrence of paradoxical effects and tolerance in other GPCR signaling pathways be explained, if not by proposing an equilibrium of opposing forces in which one signaling event triggers a negative feedback loop? This, in fact, represents a classical mechanism in signal transduction.

From our interactomic study, we identified new candidates that may trigger this counteracting antinociceptive signaling together with GPRASP1 (Fig. 6*M, N*). Indeed, only in WT mice was the association of SYNG1 with DOR further increased after a second SNC80 activation and the same was true, although to a lesser extent for the MAPkinase ERK-2, KCTD12 and UBP5. In addition, we could detect an engagement of activated DOR with a sorting nexin (either RHG33 = SNX26 or RHG32 [80,81] and with the CMIP signaling protein [82] in WT but not in GPRASP1 KO mice. Both RHG33 and RHG32 had been already detected in the interactome of Flag-DOR naive mouse midbrain [68] confirming that, in GPRASP1 KO mice, the loss of at least one of these two proteins could have functional consequences. The function of CMIP in the central nervous system remains to be explored.

Future research should focus on validating these signaling interactions in specific brain regions and cell types relevant to pain modulation. The integration of omics-based approaches may further clarify the role of GPRASP1 in cellular allostasis and help guide the development of next-generation analgesics with reduced tolerance liabilities.

While β-arrestin-biased agonists dominate drug discovery, our findings suggest alternative regulatory layers mediated by proteins like GPRASP1. Given its role in adaptation to chronic stimulation of other GPCRs, i.e. cannabinoids, dopaminergic, chemokine receptors and β2-adrenoceptors [30,36,37,40], GPRASP1 could represent a promising therapeutic target across various indications.

CRediT authorship contribution statement

Michael Dumas: Resources, Formal analysis. **Johana Chicher:** Formal analysis, Data curation. **Philippe Hammann:** Methodology, Investigation, Formal analysis, Data curation. **Juliette Kaeffer:** Writing – original draft, Visualization, Methodology, Investigation, Formal analysis, Data curation, Conceptualization. **Philippe Marin:** Writing – review & editing, Investigation, Formal analysis, Data curation. **Marie-Laure Straub:** Methodology, Investigation. **Franck Vandermoere:** Writing – review & editing, Investigation, Formal analysis, Data curation, Conceptualization. **Glenn-Marie Le Coz:** Investigation, Formal analysis. **Dominique Massotte:** Writing – review & editing, Resources, Investigation, Formal analysis, Data curation, Conceptualization. **Raphaëlle Quillet:** Investigation, Formal analysis. **Frédéric Simonin:** Writing – review & editing, Supervision, Methodology, Funding acquisition, Formal analysis, Data curation, Conceptualization. **Valérie Kugler:** Investigation, Formal analysis. **LECAT Sandra:** Writing – review & editing, Writing – original draft, Visualization, Supervision, Project administration, Methodology, Investigation, Funding acquisition, Formal analysis, Data curation, Conceptualization. **Nathalie Petit-Demoulière:** Investigation. **Manon Gerum:** Investigation. **Gabrielle Zeder-Lutz:** Resources. **Stéphane Doridot:** Resources.

Funding

This work was supported by the CNRS, LABEX Medalis (ANR-10-LABX-0034, Programme d'investissement d'avenir), Région Grand Est (19-GE6-175) and graduate school of pain EURIDOL of the University of Strasbourg (ANR- 17-EURE-0022, Programme d'investissement d'avenir) and by the SFRI- STRAT'US Project (ANR-20-SFRI-0012).

Declaration of Competing Interest

The authors declare that they have no known competing financial interests or personal relationships that could have appeared to influence the work reported in this paper.

Acknowledgements

We warmly thank the Chronobiotron, the imaging platforms at INCI and at the faculty of pharmacy of the university of Strasbourg (PIQ) and finally PCBIS platforms for technical assistance. We also thank Adam Medina for his skillful technical assistance with GPRASP1 KO mice.

Appendix A. Supporting information

Supplementary data associated with this article can be found in the online version at doi:10.1016/j.biopha.2025.118913.

Data availability

Data will be made available on request.

References

[1] S.M. Rikard, A.E. Strahan, K.M. Schmit, G.P. Guy, Prevalence of Pharmacologic and Nonpharmacologic Pain Management Therapies Among Adults With Chronic Pain-United States, 2020, Ann. Intern Med 176 (2023) 1571–1575, https://doi.org/10.7326/M23-2004.

[2] A. Fayaz, P. Croft, R.M. Langford, L.J. Donaldson, G.T. Jones, Prevalence of chronic pain in the UK: a systematic review and meta-analysis of population studies, BMJ Open 6 (2016) e010364, https://doi.org/10.1136/bmjopen-2015-010364.

[3] C.E. Zelaya, J.M. Dahlhamer, J.W. Lucas, E.M. Connor, Chronic Pain and High-impact Chronic Pain Among U.S. Adults, NCHS Data Brief. 1 (8) (2020) 2019.

[4] J. Dahlhamer, et al., Prevalence of Chronic Pain and High-Impact Chronic Pain Among Adults - United States, 2016, MMWR Morb. Mortal. Wkly Rep. 67 (2018) 1001–1006, https://doi.org/10.15585/mmwr.mm6736a2.

[5] L.S. Stone, D.C. Molliver, In search of analgesia: emerging roles of GPCRs in pain, Mol. Inter. 9 (2009) 234–251, https://doi.org/10.1124/mi.9.5.7.

[6] S. Obeng, T. Hiranita, F. León, L.R. McMahon, C.R. McCurdy, Novel Approaches, Drug Candidates, and Targets in Pain Drug Discovery, J. Med Chem. 64 (2021) 6523–6548, https://doi.org/10.1021/acs.jmedchem.1c00028.

[7] K. Humphreys, et al., Responding to the opioid crisis in North America and beyond: recommendations of the Stanford–Lancet Commission, Lancet 399 (2022) 555–604, https://doi.org/10.1016/S0140-6736(21)02252-2.

[8] N.D. Volkow, C. Blanco, The Changing Opioid Crisis: development, challenges and opportunities, Mol. Psychiatry 26 (2021) 218–233, https://doi.org/10.1038/s41380-020-0661-4.

[9] B. Quirion, F. Bergeron, V. Blais, L. Gendron, The Delta-Opioid Receptor; a Target for the Treatment of Pain, Front Mol. Neurosci. 13 (2020) 52, https://doi.org/10.3389/fnmol.2020.00052.

[10] H. Kurose, T. Katada, T. Amano, M. Ui, Specific uncoupling by islet-activating protein, pertussis toxin, of negative signal transduction via alpha-adrenergic, cholinergic, and opiate receptors in neuroblastoma x glioma hybrid cells, J. Biol. Chem. 258 (1983) 4870–4875, https://doi.org/10.1016/S0021-9258(18)32507-9.

[11] C. Gavériaux-Ruff, B.L. Kieffer, Delta opioid receptor analgesia: recent contributions from pharmacology and molecular approaches, Behav. Pharm. 22 (2011) 405–414, https://doi.org/10.1097/FBP.0b013e32834a1f2c.

[12] P. Chu Sin Chung, B.L. Kieffer, Delta opioid receptors in brain function and diseases, Pharm. Ther. 140 (2013) 112–120, https://doi.org/10.1016/j.pharmthera.2013.06.003.

[13] A.A.A. Pradhan, et al., In vivo delta opioid receptor internalization controls behavioral effects of agonists, PLoS ONE 4 (2009) e5425, https://doi.org/10.1371/journal.pone.0005425.

[14] A.A.A. Pradhan, et al., Ligand-Directed Trafficking of the δ-Opioid Receptor *In Vivo*: Two Paths Toward Analgesic Tolerance, J. Neurosci. 30 (2010) 16459–16468, https://doi.org/10.1523/JNEUROSCI.3748-10.2010.

[15] F. Khan, A. Mehan, Addressing opioid tolerance and opioid-induced hypersensitivity: Recent developments and future therapeutic strategies, Pharmacol. Res. Perspect. 9 (2021) e00789, https://doi.org/10.1002/prp2.789.

[16] C.M. Cahill, W. Walwyn, A.M.W. Taylor, A.A.A. Pradhan, C.J. Evans, Allostatic mechanisms of opioid tolerance beyond desensitization and downregulation, Trends Pharmacol. Sci. 37 (2016) 963–976, https://doi.org/10.1016/j.tips.2016.08.002.

[17] L.-A. Roeckel, G.-M. Le Coz, C. Gavériaux-Ruff, F. Simonin, Opioid-induced hyperalgesia: Cellular and molecular mechanisms, Neuroscience 338 (2016) 160–182, https://doi.org/10.1016/j.neuroscience.2016.06.029.

[18] E. Kelly, A. Conibear, G. Henderson, Biased Agonism: Lessons from Studies of Opioid Receptor Agonists, Annu. Rev. Pharmacol. Toxicol. 63 (2023) 491–515, https://doi.org/10.1146/annurev-pharmtox-052120-091058.

[19] A. Kliewer, et al., Phosphorylation-deficient G-protein-biased μ-opioid receptors improve analgesia and diminish tolerance but worsen opioid side effects, Nat. Commun. 10 (2019) 367, https://doi.org/10.1038/s41467-018-08162-1.

[20] A.A.A. Pradhan, et al., Agonist-specific recruitment of arrestin isoforms differentially modify delta opioid receptor function, J. Neurosci. 36 (2016) 3541–3551, https://doi.org/10.1523/JNEUROSCI.4124-15.2016.

[21] A. Vicente-Sanchez, et al., Tolerance to high-internalizing δ opioid receptor agonist is critically mediated by arrestin 2, BJP 175 (2018) 3050–3059, https://doi.org/10.1111/bph.14353.

[22] F. Simonin, P. Karcher, J.J.-M. Boeuf, A. Matifas, B.L. Kieffer, Identification of a novel family of G protein-coupled receptor associated sorting proteins, J. Neurochem. 89 (2004) 766–775, https://doi.org/10.1111/j.1471-4159.2004.02411.x.

[23] J.L. Whistler, et al., Modulation of Postendocytic Sorting of G Protein-Coupled Receptors, Science 297 (2002) 615–620, https://doi.org/10.1126/science.1073308.

[24] A. Heydorn, et al., A Library of 7TM Receptor C-terminal Tails: interactions with the proposed post-endocytic sorting proteins erm-binding phosphoprotein 50 (EBP50), *N* -ethylmaleimide-sensitive factor (NSF), sorting nexin 1 (SNX1), and G protein-coupled receptor-associated sorting protein(GASP), J. Biol. Chem. 279 (2004) 54291–54303, https://doi.org/10.1074/jbc.M406169200.

[25] O. Bornert, et al., Identification of a Novel Protein-Protein Interaction Motif Mediating Interaction of GPCR-Associated Sorting Proteins with G Protein-Coupled Receptors, PLoS One 8 (2013) e56336, https://doi.org/10.1371/journal.pone.0056336.

[26] S.E. Bartlett, et al., Dopamine responsiveness is regulated by targeted sorting of D2 receptors, Proc. Natl. Acad. Sci. U. S. A. 102 (2005) 11521–11526, https://doi.org/10.1073/pnas.0502418102.

[27] D. Thompson, J.L. Whistler, Dopamine D3 receptors are down-regulated following heterologous endocytosis by a specific interaction with G protein-coupled receptor-associated sorting protein-1, J. Biol. Chem. 286 (2011) 1598–1608, https://doi.org/10.1074/jbc.M110.158345.

[28] A. Marley, M. Von Zastrow, Dysbindin Promotes the Post-Endocytic Sorting of G Protein-Coupled Receptors to Lysosomes, PLoS ONE 5 (2010) e9325, https://doi.org/10.1371/journal.pone.0009325.

[29] S. Rosciglione, C. Theriault, M.-O. Boily, M. Paquette, C. Lavoie, Gas regulates the post-endocytic sorting of G protein-coupled receptors, Nat. Commun. 5 (2014) 1–11, https://doi.org/10.1038/ncomms5556.

[30] L. Martini, et al., Ligand-induced down-regulation of the cannabinoid 1 receptor is mediated by the G-protein-coupled receptor-associated sorting protein GASP1, FASEB J. 21 (2007) 802–811, https://doi.org/10.1096/fj.06-7132com.

[31] A. Tappe-Theodor, et al., A Molecular Basis of Analgesic Tolerance to Cannabinoids, J. Neurosci. 27 (2007) 4165–4177, https://doi.org/10.1523/JNEUROSCI.5648-06.2007.

[32] C. He, et al., Beclin 2 Functions in Autophagy, Degradation of G Protein-Coupled Receptors, and Metabolism, Cell 154 (2013) 1085–1099, https://doi.org/10.1016/j.cell.2013.07.035.

[33] K. Kuramoto, et al., Autophagy activation by novel inducers prevents BECN2-mediated drug tolerance to cannabinoids, Autophagy 12 (2016) 1460–1471, https://doi.org/10.1080/15548627.2016.1187367.

[34] A. Abu-Helo, F. Simonin, Identification and biological significance of G protein-coupled receptor associated sorting proteins (GASPs), Pharm. Ther. 126 (2010) 244–250, https://doi.org/10.1016/j.pharmthera.2010.03.004.

[35] J. Kaeffer, G. Zeder-Lutz, F. Simonin, S. Lecat, GPRASP/ARMCX protein family: potential involvement in health and diseases revealed by their novel interacting partners, Curr. Top. Med Chem. 21 (2021) 227–254, https://doi.org/10.2174/1568026620666201202102448.

[36] J. Boeuf, et al., Attenuated behavioural responses to acute and chronic cocaine in GASP-1-deficient mice, Eur. J. Neurosci. 30 (2009) 860–868, https://doi.org/10.1111/j.1460-9568.2009.06865.x.

[37] D. Thompson, L. Martini, J.L. Whistler, Altered ratio of D1 and D2 dopamine receptors in mouse striatum is associated with behavioral sensitization to cocaine, PLoS One 5 (2010) e11038, https://doi.org/10.1371/journal.pone.0011038.

[38] S. Schamiloglu, et al., Arrestin-3 Agonism at Dopamine D3 Receptors Defines a Subclass of Second-Generation Antipsychotics That Promotes Drug Tolerance, –2, Biol. Psychiatry S0006-3223 (23) (2023) 01092, https://doi.org/10.1016/j.biopsych.2023.03.006. –2.

[39] R. Li, et al., GPRASP1 loss-of-function links to arteriovenous malformations by endothelial activating GPR4 signals, Brain 147 (2024) 1571–1586, https://doi.org/10.1093/brain/awad335.

[40] A. Abu-Helo, et al., GPRASP1 deletion in mice abrogates adverse side effects associated with chronic stimulation of Beta2-adrenoceptor, Biomed. Pharmacother. 187 (2025) 118073, https://doi.org/10.1016/j.biopha.2025.118073.

[41] L. Martini, D. Thompson, V. Kharazia, J.L. Whistler, Differential Regulation of Behavioral Tolerance to WIN55,212-2 by GASP1, Neuropsychopharmacol 35 (2010) 1363–1373, https://doi.org/10.1038/npp.2010.6.

[42] G. Scherrer, et al., Knockin mice expressing fluorescent delta-opioid receptors uncover G protein-coupled receptor dynamics in vivo, Proc. Natl. Acad. Sci. USA 103 (2006) 9691–9696, https://doi.org/10.1073/pnas.0603359103.

[43] L. Faget, et al., In vivo visualization of delta opioid receptors upon physiological activation uncovers a distinct internalization profile, J. Neurosci. 32 (2012) 7301–7310, https://doi.org/10.1523/JNEUROSCI.0185-12.2012.

[44] E. Erbs, et al., A mu-delta opioid receptor brain atlas reveals neuronal co-occurrence in subcortical networks, Brain Struct. Funct. 220 (2015) 677–702, https://doi.org/10.1007/s00429-014-0717-9.

[45] A.A.A. Pradhan, V.L. Tawfik, A.F. Tipton, G. Scherrer, In Vivo Techniques to Investigate the Internalization Profile of Opioid Receptors, Methods Mol. Biol. 1230 (2015) 87–104, https://doi.org/10.1007/978-1-4939-1708-2_7.

[46] Z. Seltzer, R. Dubner, Y. Shir, A novel behavioral model of neuropathic pain disorders produced in rats by partial sciatic nerve injury, PAIN 43 (1990) 205, https://doi.org/10.1016/0304-3959(90)91074-S.

[47] S.R. Chaplan, et al., Quantitative assessment of tactile allodynia in the rat paw, J. Neurosci. Methods 53 (1994) 55–63, https://doi.org/10.1016/0165-0270(94)90144-9.

[48] Y. Xue, et al., The Human SCN9A^{R185H} Point Mutation Induces Pain Hypersensitivity and Spontaneous Pain in Mice, Front. Mol. Neurosci. 15 (2022) 913990, https://doi.org/10.3389/fnmol.2022.913990.

[49] L.A. Roeckel, et al., Morphine-induced hyperalgesia involves mu opioid receptors and the metabolite morphine-3-glucuronide, Sci. Rep. 7 (2017) 10406, https://doi.org/10.1038/s41598-017-11120-4.

[50] A. Drieu la Rochelle, et al., A bifunctional biased mu opioid agonist-neuropeptide FF receptor antagonist as analgesic w ith improved acute and chronic side effects, Pain 159 (9) (2018) 1705–1718, https://doi.org/10.1097/j.pain.0000000000001262.

[51] A. Vicente-Sanchez, L. Segura, Pradhan, A.A. The delta opioid receptor tool box, Neuroscience 338 (2016) 145–159, https://doi.org/10.1016/j.neuroscience.2016.06.028.

[52] R.E. Sorge, et al., Different immune cells mediate mechanical pain hypersensitivity in male and female mice, Nat. Neurosci. 18 (2015) 1081–1083.

[53] Mapplebeck, et al., Chloride Dysregulation through Downregulation of KCC2 Mediates Neuropathic Pain in Both Sexes, Cell Rep. 28 (2019) 590–596, https://doi.org/10.1016/j.celrep.2019.06.059.

[54] D. Reiss, et al., Delta Opioid Receptor in Astrocytes Contributes to Neuropathic Cold Pain and Analgesic Tolerance in Female Mice, Front. Cell. Neurosci. 15 (2021) 745178, https://doi.org/10.3389/fncel.2021.745178.

[55] M. Kremer, et al., Antidepressants and gabapentinoids in neuropathic pain: Mechanistic insights, Neuroscience 338 (2016) 183–206, https://doi.org/10.1016/j.neuroscience.2016.06.057.

[56] E. Erbs, et al., Impact of chronic morphine on delta opioid receptor expressing neurons in the mouse hippocampus, Neuroscience 313 (2016) 46–56, https://doi.org/10.1016/j.neuroscience.2015.10.022.

[57] Q. Wang, et al., V-ATPase modulates exocytosis in neuroendocrine cells through the activation of the ARNO-Arf6-PLD pathway and the synthesis of phosphatidic acid, Front Mol. Biosci. 10 (2023) 1163545, https://doi.org/10.3389/fmolb.2023.1163545.

[58] O.M. Kouhen, et al., Hierarchical phosphorylation of delta-opioid receptor regulates agonist-induced receptor desensitization and internalization, J. Biol. Chem. 275 (2000) 36659–36664, https://doi.org/10.1074/jbc.M006788200.

[59] A. Mann, et al., Agonist-induced phosphorylation bar code and differential post-activation signaling of the delta opioid receptor revealed by phosphosite-specific antibodies, Sci. Rep. 10 (2020) 8585, https://doi.org/10.1038/s41598-020-65589-7.

[60] C.E. Philibert, et al., TrkB receptor interacts with $mGlu_2$ receptor and mediates antipsychotic-like effects of $mGlu_2$ receptor activation in the mouse, Sci. Adv. 10 (2024) eadg1679, https://doi.org/10.1126/sciadv.adg1679.
[61] G. Zeder-Lutz, et al., Characterization of anti-GASP motif antibodies that inhibit the interaction between GPRASP1 and G protein-coupled receptors, Anal. Biochem 665 (2023) 115062, https://doi.org/10.1016/j.ab.2023.115062.
[62] A.T. Blaine, R.M. van Rijn, Receptor expression and signaling properties in the brain, and structural ligand motifs that contributes to delta opioid receptor agonist-induced seizures, Neuropharmacology 232 (2023) 109526, https://doi.org/10.1016/j.neuropharm.2023.109526.
[63] T. Laboute, et al., Orphan receptor GPR158 serves as a metabotropic glycine receptor: mGlyR, Science 379 (2023) 1352–1358, https://doi.org/10.1126/science.add7150.
[64] E. Diaz, Beyond the AMPA receptor: Diverse roles of SynDIG/ PRRT brain-specific transmembrane proteins at excitatory synapses, Curr. Opin. Pharmacol. 58 (2021) 76–82, https://doi.org/10.1016/j.coph.2021.03.011.
[65] D. Jullié, C. Benitez, T.A. Knight, M.S. Simic, M. von Zastrow, Endocytic trafficking determines cellular tolerance of presynaptic opioid signaling, Elife 11 (2022) e81298, https://doi.org/10.7554/eLife.81298.
[66] B.T. Lobingier, et al., An Approach to Spatiotemporally Resolve Protein Interaction Networks in Living Cells, Cell 169 (2017) 350–360, https://doi.org/10.1016/j.cell.2017.03.022.
[67] B. Novy, et al., An engineered trafficking biosensor reveals a role for DNAJC13 in DOR downregulation, Nat. Chem. Biol. (2024), https://doi.org/10.1038/s41589-024-01705-2.
[68] J. Degrandmaison, et al., In vivo mapping of a GPCR interactome using knockin mice, Proc. Natl. Acad. Sci. USA 117 (2020) 13105–13116, https://doi.org/10.1073/pnas.1917906117.
[69] E.L. Gorenberg, S.S. Chandra, The Role of Co-chaperones in Synaptic Proteostasis and Neurodegenerative Disease, Front. Neurosci. 11 (2017) 248, https://doi.org/10.3389/fnins.2017.00248.
[70] B.J. Polacco, et al., Profiling the proximal proteome of the activated μ-opioid receptor, Nat. Chem. Biol. (2024), https://doi.org/10.1038/s41589-024-01588-3.
[71] V.M. Gadotti, et al., Small organic molecule disruptors of Cav3.2 - USP5 interactions reverse inflammatory and neuropathic pain, Mol. Pain. 11 (2015) 12, https://doi.org/10.1186/s12990-015-0011-8.
[72] A. Peretz, A, et al., Hypomyelination and increased activity of voltage- gated K^+ channels in mice lacking protein tyrosine phosphatase e. *EMBOJ* 19 (2000) 4036–4045, https://doi.org/10.1093/emboj/19.15.4036.
[73] L. Gendron, C.M. Cahill, M. von Zastrow, P.W. Schiller, G. Pineyro, Molecular Pharmacology of d-Opioid Receptors, Pharm. Rev. 68 (2016) 631–700, https://doi.org/10.1124/pr.114.008979.
[74] P.A. Colussi, C.H. Taron, J.C. Mack, P. Orlean, Human and *Saccharomyces cerevisiae* dolichol phosphate mannose synthases represent two classes of the enzyme, but both function in *Schizosaccharomyces pombe*, Proc. Natl. Acad. Sci. USA 94 (1997) 7873–7878, https://doi.org/10.1073/pnas.94.15.7873.
[75] C.J. Smith, D.M. Berry, C.J. McGlade, The E3 ubiquitin ligases RNF126 and Rabring7 regulate endosomal sorting of the epidermal growth factor receptor, J. Cell Sci. 126 13661380 (2013), https://doi.org/10.1242/jcs.116129.
[76] M. Stoeber, et al., A genetically encoded biosensor reveals location bias of opioid drug action, Neuron 98 (2018) 963–976.e5, https://doi.org/10.1016/j.neuron.2018.04.021.
[77] N.N. Jimenez-Vargas, et al., Endosomal signaling of delta opioid receptors is an endogenous mechanism and therapeutic target for relief from inflammatory pain, Proc. Natl. Acad. Sci. U. S. A. 117 (2020) 15281–15292, https://doi.org/10.1073/pnas.2000500117.
[78] P. Tschische, et al., The G-protein Coupled Receptor Associated Sorting Protein GASP-1 Regulates the Signaling and Trafficking of the Viral Chemokine Receptor US28, Traffic 11 (2010) 660–674, https://doi.org/10.1111/j.1600-0854.2010.1045.x.
[79] T. Buenaventura, et al., A Targeted RNAi Screen Identifies Endocytic Trafficking Factors That Control GLP-1 Receptor Signaling in Pancreatic β-Cells, Diabetes 67 (2018) 385–399, https://doi.org/10.2337/db17-0639.
[80] T. Nakazawa, et al., Emerging roles of ARHGAP33 in intracellular trafficking of TrkB and pathophysiology of neuropsychiatric disorders, Nat. Commun. 7 (2015) 10594, https://doi.org/10.1038/ncomms10594.
[81] J. Diring, S. Mouilleron, N.Q. McDonald, R. Treisman, RPEL-family rhoGAPs link Rac/Cdc42 GTP loading to G-actin availability, Nat. Cell Biol. 21 (2019) 845–855, https://doi.org/10.1038/s41556-019-0337-y.
[82] M. Ollero, D. Sahali, The Enigmatic Emerging Role of the C-Maf Inducing Protein in Cancer, Diagnostics 11 (2021) 666, https://doi.org/10.3390/diagnostics11040666.

Glossary

AP-MS: Affinity-Purification-Mass Spectrometry
CCI: chronic constriction injury
CFA: Complete Freund Adjuvant
CP: cold plate
DOR: Delta-opioid receptor
eGFP: enhanced Green Fluorescent Protein
GPCRs: G-protein coupled receptors
GPRASP1: GPCR associated sorting protein 1
KI: Knock-In
KO: Knock-Out
LFQ: Label Free Quantification
MS: Mass Spectrometry
Nti: Naltrindole
TPT: tail pressure test
TIT: tail immersion test; VF, von Frey